ABSTRACT

Title of Document:	SILANE CROSS-LINKED GRAPHENE OXIDE MEMBRANE DEMONSTRATING UNIQUE TRANSPORT PHENOMENA IN AQEOUS PHASE SEPARATION
	Sunxiang Zheng, Master of Science, 2015
Directed By:	Assistant Professor, Dr. Baoxia Mi Department of civil & Environmental Engineering

Graphene oxide (GO) membranes are considered promising for water purification applications. We synthesized a novel GO membrane using inorganic silane as a cross linker. Briefly, a pH 3 GO solution was filtrated through polyethersulfone (PES) membrane supports by vacuum filtration. The GO layers deposited on the PES supports were subsequently soaked in a saturated sodium metasilicate solution for

crosslinking and stabilization. As a final step, the readily stabilized GO membranes were transferred into a 10% H_2SO_4 solution for further stabilization. The GO membrane exhibits unique rejection properties to uncharged organic species (~ 85%) and ionic species (~6%). A high water flux of 39 $L/m^2/h$ and a reasonable back solute flux of 0.011 $mol/m^2/h$ were observed with 0.25M trisodium citrate dehydrate (TSC) as draw solution in forward osmosis (FO). The GO membrane also demonstrates some interesting Janus effects and enables directional water gating (by blocking the permeation in one direction while allowing the permeation in the other direction).

SILANE CROSS-LINKED GRAPHENE OXIDE MEMBRANE
DEMONSTRATING UNIQUE TRANSPORT PHENOMENA
IN AQUEOUS PHASE SEPARATION

By

Sunxiang Zheng

Thesis submitted to the Faculty of the Graduate School of the
University of Maryland, College Park, in partial fulfillment
of the requirements for the degree of
Master of Science
2015

Advisory Committee:
Professor Dr. Baoxia Mi, Chair
Professor Dr. Alba Torrents
Professor Dr. Allen P. Davis

Dedication

TO

My Grandma and Late Grandpa

And

My Dad and Mum

Acknowledgements

I would like to give my sincere appreciation and gratitude to my advisor Dr. Baoxia Mi for all her help and knowledge during the past two years. Her support and guidance were vital throughout this course of work. I'm also grateful to the other committee members, Dr. Alba Torrents and Dr. Allen P. Davis for the inspirational lectures during my academic years and their participation in my thesis evaluation.

Special thanks also go to my colleagues from Membrane Innovation Lab at University of Maryland: Dr. Meng Hu, Dr. Qian Yang, Yan Kang, Yoontaek Oh, Alisha Chan and Dr. Limei Jing.

At last, I want to thank the support and encouragement from my friends and my parents. Any achievement I get now is based on their care and help in my daily life and previous education.

Table of Contents

List of Tables

List of Figures

Chapter 1: Introduction

1.1 Research Background

Water scarcity has been listed as one of the major problems the human kinds need to face in the very near future. The US federal and local agencies have spent decades supporting and encouraging researchers to exploit possible solutions for desalination and purifying impaired water. As a relatively new material, layered graphene oxide (GO) forms nanochannels that are advantageous to generate fast water transport while maintaining good solute rejection. However, to utilize the advantages of GO material, it is critical to develop facile, highly scalable GO-based membranes and understand their separation mechanisms in various applications. Therefore, this research is meant to optimize the synthesis of GO membranes and find widespread applications such as point-of-use water purification, on-site treatment of hydrofracking flowback water, renewable energy production, and drug delivery and artificial organ development.

1.2 Study objectives

The purpose of this study was to introduce the inorganic silane as a cross-linker to stabilize the laminated graphene oxide (GO) layers in an aqueous environment for GO membrane fabrication and test the membranes performance in both pressurized filtration system and lab-scaled forward osmosis (FO) system. The specific research objectives are:

1. To exploit a novel approach for fabricating a silane cross-linked GO membrane using dehydration and gelation chemistry. The successful cross-linking reaction was proved by characterization techniques such as Fourier transform infrared spectroscopy (FTIR) and X-ray photoelectron spectroscopy (XPS).

2. To characterize the membrane structural and compositional properties by visional analysis techniques such as scanning electron microscope (SEM) and Transmission electron microscopy (TEM) and quantitative analysis techniques such as Energy dispersive spectroscopy (EDS).

3. To evaluate the membrane performance in both pressurized filtration system and lab-scaled FO system.

4. To fundamentally understand the water and solute transport mechanisms based on the previous characterization and performance test results.

1.3 Thesis structure

This course of work was composited to synthesize and evaluate the silane cross-linked GO membranes. The rest of the chapters are constructed and organized as the following:

Chapter 2 reviews the development of membrane technology, the concept of forward osmosis, physiochemical properties of GO, different synthesis approaches of GO and the current stage of incorporating GO for various membrane materials.

Chapter 3 provides the materials and methods used for membrane fabrication, characterization and performance tests.

Chapter 4 discusses the results from the membrane characterization and performance tests.

Chapter 5 is a summary of the entire work, and states the implications and future work based on the preliminary results.

Chapter 2: Literature Review

2.1 Membrane technology

In the past few decades, the expending global population and economies had repeatedly brought the world water demand to a new level [1-5]. Regionally, the water consumption for either domestic or industrial need has overwhelmed the fresh water production capacity. An announcement made by the World Water Council predicted that by 2030, 3.9 billion people will be in regions characterized as "water scarce" [6]. On the other hand, environmental pollution is increasingly becoming a serious problem worldwide. Our limited water resources deteriorated significantly and will not be easily recovered in the very near future. More than ever, an efficient and sustainable water production and treatment technology is needed as we turn into the 21th century. Membranes are favored because of its wide applications, which meet the need of both fresh water production and environmental protection.

Membrane technology started as the concept of "osmosis" was firstly proposed in 1748 by a French cleric J. Abbe Nollet. The foundational development took about 200 years until the first asymmetric membrane was synthesized in 1962, which made commencement of practical membrane applications. Ever since, the membrane technology began to thrive and developed in various perspectives.

Microfiltration (MF), ultrafiltration (UF), nanofiltration (NF), and reverse osmosis (RO) membranes are types of pressure-driven membranes with the pore size ranging from several micrometers to less than one nanometer [7-11]. Membranes with

different pore sizes are considered to be capable of removing certain types of "contaminates" in the water due to the size exclusive transport mechanism [12-15]. Figure 2.1 gives an estimation of the possible removal of undesired compounds by membranes ranging from microfiltration to reverse osmosis.
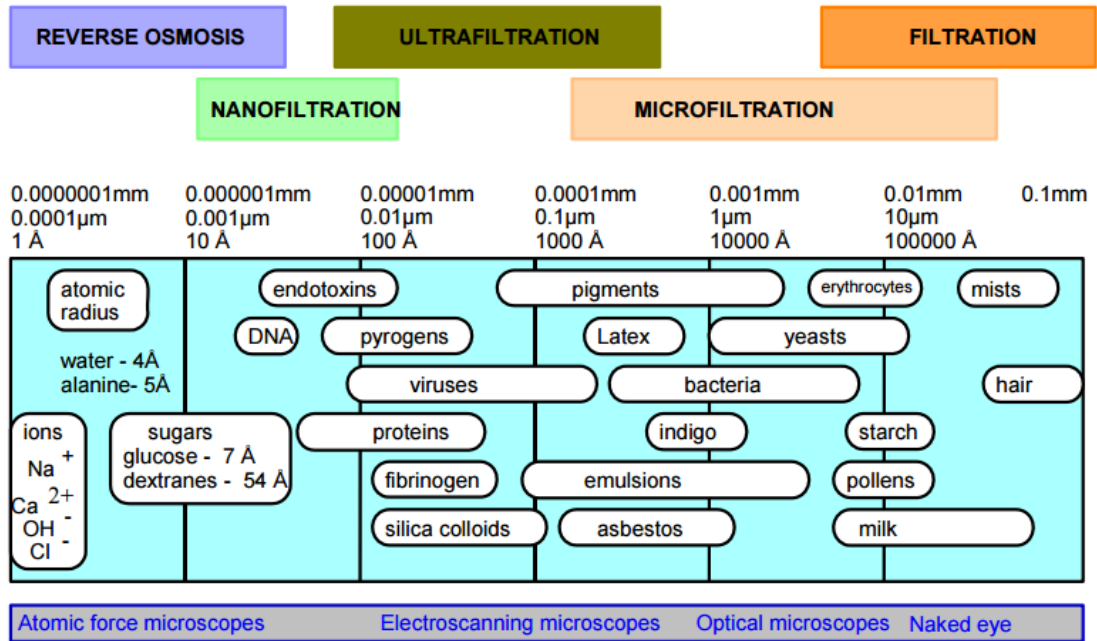
Figure 2.1 The separation processes of pressure-driven membranes (Kabsch-Korbutowicz and Kutylowska 2008)

Membranes can be composited by different materials, among which polymeric membranes and inorganic membranes are widely used in separation processes such as water purification, protein separation, metal recovery, and pigment recovery [8].

Inorganic membranes were developed and applied for mass separation in 1980's [16-18]. Ceramic membranes as a representative kind of inorganic membranes have asymmetric structure with denser top layers and more porous bottom layers [19-21]. Materials such as alumina, silica, zeolite, and porous metals were studied and used for

ceramic membrane fabrication [22-25]. This sort of membrane has advantages such as enhanced mechanical properties, good thermal and chemical stability, and high resistance to membrane fouling. It has been proved that ceramic membranes have a longer lifetime and higher fouling duration than most of the polymeric membranes. With that, inorganic membranes are usually applied in heavy-duty separation processes such as in petroleum industries.

The porous polymeric membranes, which are the most commonly used MF and UF membranes, are intensively used in water treatment processes. These membranes also have asymmetric structures with a less porous skin layer on the one side and a nearly non-selective support layer on the other side [8, 11, 26]. In water filtration and separation processes, the skin layer acts as a "filter" that allows the water molecule to pass through while rejecting the targeted compounds. This procedure is usually pressure driven and the driving force is proportional to the water flux. Consequently, in order to achieve a desired filtration rate, water purification using UF/MF membranes is also very energy intensive. Another concern for the polymeric UF/MF membranes is the relevantly low resistance to the membrane fouling issues [27-31]. Foulants can easily attach to the membrane surface and cause a significant decrease in membrane permeability. Moreover, after a long period of running, it becomes hard to completely remove the foulants by traditional washing processes.

With the rapid development of nanotechnology, nanomaterials have been incorporated into membranes to optimize the pore size and enhance the overall performance. NF membranes and RO membranes were therefore developed to remove even smaller compounds in the water.

The NF membranes have properties between UF membranes and RO membranes [32-37] with advantages such as relevantly low operation pressure, high rejection of multivalent anion salts, and high water flux. Additionally, NF membranes can be easily functionalized with multiple functional groups (e.g. carboxylic and sulfonic groups). As a result, the membrane have a charged surface, which provide extra repulsion to the ionic species due to the charge screening effect [38-41].

The RO membranes were designed with pore size less than one nanometer to remove the monovalent salts [11, 42-44]. Generally, RO membranes have three layers [43, 45-51]. From the bottom to the top, a support layer (e.g. Polyester) with high mechanical strength forms the basal plane of the membrane, which then is covered by MF/UF membrane (e.g. Polyethersulfone) as a second layer. On the top, there is a nanometer-thick selective layer (e.g. Polyamide).

Over the past few decades, incredible improvements have been made in fabrication and modification of RO membranes. Now, RO is the leading desalination technology with one fifth of energy consumption and one tenth of the operation cost compared to those in 1970's [52].

Seven-fold higher water permeability and salt rejection have been achieved due to the remarkable progresses in membrane materials and fabrication methods. It has overtaken conventional thermal technology such as multi-stage flash (MSF) and is still keeping in growth. Nevertheless, the commercialized RO membranes still suffer from problems like low chlorine duration and poor anti-fouling property. Thus, new RO membrane materials and other desalination methods are still highly desirable.

2.2 Forward Osmosis

The concept of forward osmosis (FO) derived from the natural osmosis phenomenon [53, 54]. In fact, within the human's body, the mass transportation through a cell's membrane is partially driven by the osmotic pressure difference. Briefly, the dissolved molecules or ions can generate a certain amount of osmotic pressure as shown in Equation 1.

$$\pi = ncRT \tag{1}$$

Where, n is the number of dissolved species,

c is the concentration of each species,

R is the ideal gas constant, and

T is the temperature.

Water tends to go through the semi-permeable membrane to the side that has higher osmotic pressure [1, 55-57].

Forward osmosis membranes take advantages of the osmotic pressure difference across the membrane, rather than hydraulic pressure difference (as in RO) as the driving force. Ideally, a concentrated draw solution which generates higher osmotic pressure than the natural sea water could draw the water molecule passing through the semi-permeable FO membrane leaving salts in the feed solution. Furthermore, instead of concentration gradient, FO process could also be driven by the thermal gradient. In this case, energy like industrial waste heat and geothermal energy can be utilized for water purification. Hence, FO is considered as a more sustainable alternative to the RO processes in desalination.

Water transportation in FO can be described as:

$$J_w = A(\Delta\pi - \Delta P) \tag{2}$$

Where, J_w is the water flux,

A is the water permeability constant,

ΔP is the applied pressure.

Pressure retarded osmosis (PRO) is in between FO and RO, where a hydraulic pressure is applied against the osmotic pressure gradient and water flux direction [58-61]. A unique application for PRO process is energy production. In theory, the maximum energy that can be extracted during the reversible mixing of a dilute feed solution and a concentrated draw solution ranges from 0.75 KWh per cubic meter to 14.1 KWh per cubic meter [4]. However, neither of the FO and PRO can achieve the theoretical working condition because of the limitation of membrane materials and the significant concentration polarization effect [62].

The modern applications of FO and PRO include and not limit to wastewater treatment, potable reuse for life support systems, water purification (e.g. hydration bags), desalination, food[63] processing, and pharmaceutical delivery [3, 63-67].

2.3 Graphene Oxide

2.3.1 Morphology and Structure

Graphene oxide (GO) is the oxidized form of graphene, which is a one atomic thick monoplane. The atomic structure of GO has been studied over 40 years, and yet no unambiguous model exists [68].
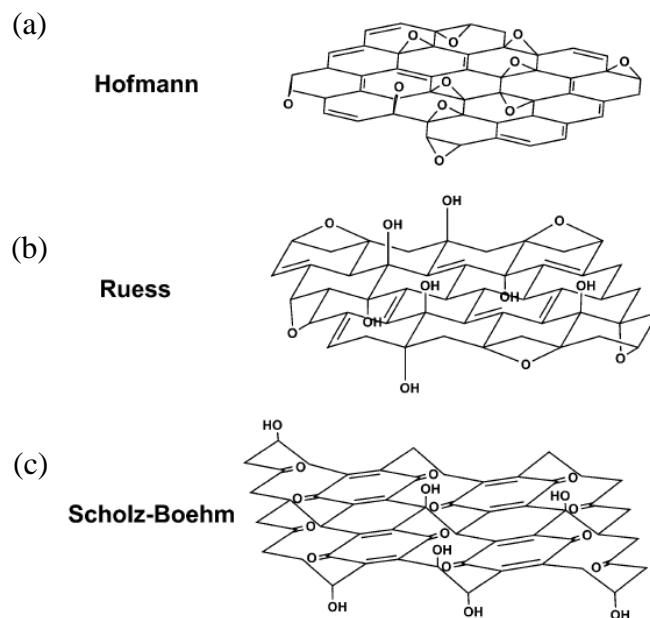
Figure 2.2 Historical development of GO structural model [68]

Among the earlier stage of researches, Hofmann's model proposed a lattices structure surrounding by epoxide groups (Figure 2.2 (a)), with a molecular formula of C_2O [69]. Ruess's model came out in 1946, altered the flat plane to a sp3 hybridized structure with both epoxide and hydroxyl groups [70] (Figure 2.2 (b)). Later on, in 1969 Scholz and Boehm's model went back from the sp3 hybridized structure to sp2 hybridized structure (Figure 2.2 (c)). However, in their suggestion, all the epoxide groups were removed, substituting with regular quinoidal species in a corrugated backbone [71].

The most recent and widely adopted GO model is the one suggested by Lerf and Klinowski. This model rejected the previous lattice structure and focused on a nonstoichiometric, amorphous alternative [72].
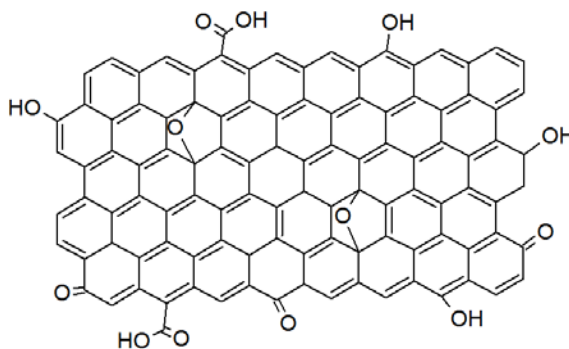
Figure 2.3 Lerf Klinowski model of GO nanosheet

Generally, the aromatic honeycomb lattice decorating with epoxide groups, carboxyl groups and double bonds are isolated from each other in variable sizes ranging from few micrometers to tens of nanometers in diameter (Figure 2.3). Single GO nanosheets can have defects such as topological defects (e.g., pentagons, heptagons, or their combination), vacancies, edges/cracks, adsorbed impurities [73].

2.3.2 Synthesis of Graphene Oxide

Although the massive production of graphene has not been realized yet, GO can be synthesized through simple chemical exfoliation by using inexpensive graphite as a raw material.

The earliest experimentally method for GO oxidation was discovered and improved by British chemist B. C. Brodie. Briefly, potassium chlorate ($KClO_3$) was used with the addition of nitric acid (HNO_3) as the oxidation agent. With heating and vigorous stirring, the oxidation product termed as graphitic acid was dissolved. The final steps included the separation of inoxidized graphite residue via filtration, the

multiple washing procedures, and the sonication [74]. In his research, Brodie analyzed the chemical composition after the first oxidation and found difference after up to four times oxidation. The final carbon, hydrogen, oxygen ratio was stabilized at around 61.04:1.85:37.11 [68].

Another remarkable synthesis approach that invented 40 years later was named after L. Staudenmaier. In his method, sulfuric acid was added to increase the acidity of the mixture. Yet, this simple change to Brodie's method resulted in a significant improvement in GO oxidation level.

The most recent GO synthesis method was proposed by Hummers and Offeman about 60 years later than Staudenmaier. Potassium permanganate ($KMnO_4$) was used as an alternative oxidation agent, which could achieve an even higher oxidation level. Ever since, several modified Hummer's methods have been suggested, yet slight changes have been made.

2.3.3 Graphene Oxide Enabled Membranes

The unique physiochemical properties of GO can be applied in different fields. Graphene and graphene oxide were first applied in the material engineering due to their good electrical conductivity. Later on, due to its facile and one atomic thick structure, the idea of using a single layer of graphene as a membrane filter was proposed. Technology development in chemical vapor deposition (CVD) has largely improved the size of graphene that can be produced. However, the difficulties of manipulating the graphene at atomic lever have not yet been overcome. The procedure is still very expensive and inefficient.

As proposed by R.R. Nair et al. in 2012 [75], the laminated GO can only allow the passage of water molecules while rejecting dissolved molecules and ions. This study brought up new opportunities for using the readily accessible GO as a new membrane material. Theoretically, laminated GO layers are stacked parallelly to each other termed as GO nanochannels [76, 77]. Different from the traditional asymmetric thin film membrane which has perpendicular water channels, GO membrane intends to create a detoured water path, which could increase the retention capacity and hence increase the membrane selectivity. The surface decoration of all the oxygenated functional groups makes GO an extremely hydrophilic material, which enables the water to slip through with nearly no friction. Recently, some studies [76, 78] have pointed out that water molecules have ultrafast transport on the inoxidized graphitic plane whereas the oxygenated functional groups created enough interlayer space for water passage. Yet, the validation of this theory needs to be resolved by further investigation.

Despite of the high water permeability and selectivity, GO membranes are believed to have outstanding antifouling properties [79, 80]. The layered structure of GO is beneficial to reject potential foulants as it forms a 2D barrier. The hydrophilicity helps to prevent the hydrophobic particles from attaching and blocking the membrane surface. Moreover, GO was reported to be toxic to most of the microbial. In this case GO membrane is anticipated to have good anti-biofouling property [81-83].

In addition, because of its high abundance of oxygenated functional groups and its aromatic carbon structure, GO nanosheet has unique interactions with heavy metals

and organic molecules. Briefly, the 2-dimessional GO nanosheet has large surface area, which makes it a good adsorbent. There are two main mechanism that have been proposed to illustrate the adsorption of aromatic organics on GO, named as the π-π dispersion interaction, and the electron donor-acceptor complex. The first mechanism was proposed by Coughlin and Ezra, who later on proved their theory by observing a decrease in adsorption with a more oxidized carbon basal plane. In their theory, the oxygenated groups remove electrons from the π-electron system, creating positive holes in the conducting π-band of the graphitic planes. Consequently, it lowers the interactions between the π-electrons of the GO and the π-electrons from the aromatic organics.

The second mechanism suggested by Mattson and his colleagues mainly focused on the electron transfer between the organics and GO. The hypothesis suggested that the carbonyl oxygen of the GO surface can act as the electron donor and the aromatic carbon of the GO can act as the accepter.

As the previous research have been focused on the adsorption kinetics between GO and the organics, the hindered diffusion mechanism in GO nanochannels has not yet been well studied. The π-π dispersion interaction was thought to increase diffusion resistance of the aromatic organics, which could potentially lead to a high rejection of this type of molecules. Moreover, the extreme hydrophilicity of GO would also help to lower the diffusivity of organic molecules. To date, in water purification applications, GO membranes have been used to remove arsenics [84, 85], pesticides[86-88], humid acid[89] and pharmaceuticals[90-92].

A great challenge for GO-enabled membrane is that GO layers tend to swell and disperse into the aqueous solution due to its extreme hydrophilicity. Consequently, the stabilization of GO layers was considered as the first step toward the success of synthesizing high performance GO membranes. So far, there are mainly two strategies [93]. Layer-by-layer (LbL) assembly via electrostatic interactions between the positively charged electrolytes and the negatively charged GO has been applied in many researches [80, 94, 95]. However, recent studies have pointed out that the LbL GO membranes are not stable in surfactants and high ionic strength environment [96]. Concerns are the inevitable and irreversible loss of GO and electrolyte layers [97]. A second approach is to cross link the GO layers by using the proper cross-linkers. Since covalent bindings are more stable than the charge interaction, cross-linked GO membranes have relevantly higher water stability.

Works have been done using amine contained monomers and polymers to cross link GO layers [98-100]. A huge advantage is that the reaction could be done in an organic solvent, which prevent the resuspension of GO nanosheets. On the other hand, drawbacks of using these cross-linkers include the relevant large interlayer spacing and the increase in hydrophobicity.

Compared to the traditional organic cross-linker, inorganic cross-linkers usually have higher hydrophilicity and better chemical stability. However, most of the available inorganic cross-linkers are extremely insoluble in the organic solvent. Prior to this study, research have been done on synthesizing GO-inorganics nanocomposite membranes. Yet, the laminal GO membrane cross-linked by the inorganics has not been well studied. A major challenge was to cross link GO layers in an aqueous

15

solution while maintain the laminal structure of GO layers. Herein, we proposed a novel GO membrane cross-linked by the inorganic and inexpensive silica gel.

Chapter 3: Material and Methods

3.1 Materials

The chemicals that were used in this course of work and their manufacturers are listed in Table 3.1. All the chemicals were used as they were purchased unless noted otherwise.

Table 3.1 Manufacturer and specification of experimental chemicals

Items	Manufacturer	specification
Graphite	Sigma-Alorich	
Sodium Nitrate (NaNO$_3$)	Sigma-Alorich	≥99.0%
Potassium Permagnate (KMnO$_4$)	Sigma-Alorich	Powder,~325 mesh
Sulfuric Acid (H$_2$SO$_4$)	BDH Chemicals	95.0~98.25% min
Hydrochloric Acid (HCl)	BDH Chemicals	36.5~38.0% min
Sodium Metasilicate (Na$_2$O$_3$Si)	Sigma-Alorich	Mw: 122.06
Sodium Chloride (NaCl)	EMD Chemicals	
Sodium Sulfate (Na$_2$SO$_4$)	Sigma-Alorich	≥99.0%, anhy powder
Magnesium Chloride (MgCl$_2$)	Sigma-Alorich	≥98.0%
Trisodium Citrate Dihydrate (TSC)	Alfa Aesar	FW:294.1(258.07 anhy)
Sucrose	Fisher Science Edu.	
Glucose	Sigma-Alorich	Mw:180.16
Poly(ethlylene glycol) (PEG)	Sigma-Alorich	Mw~1500
Poly(allylanmine hydrochloride) (PAH)	Sigma-Alorich	Mw~15000
Polyethersulfone Membrane (PES)	Sterlitech Corporation	Average pore size ~ 0.3μm

3.2 GO Preparation

Suspended GO aqueous solution was prepared by using modified Hummers method [73, 93, 101]. Firstly, 5g of powdered flake graphite, 2.5g of $NaNO_3$, and 115mL of sulfuric acid were added into a 1-L flask, which was sitting in an ice bath to prevent over-heating and potential explosion. 15g of $KMnO_4$ was subsequently added into the mixture while mixing vigorously by magnetic stirring. Then, the flask was transferred to a 35°C water bath for 30 min before another transfer to a 98°C water bath. Roughly 230 mL deionized (DI) water was added to the mixture at this time. The resulting pasty solution was diluted to approximately 0.7 L after cooling down to room temperature. We added 5mL of 30% H_2O_2 to further oxidize the graphitic acid. The final solution was filtered through a PET fiber for washing and purification.

To purify the GO solution, we first centrifuge the filtrate at 6450 rpm for 2 h, and decanted the supernatant. The GO precipitation was washed through four circles of resuspension and centrifuge using DI, 30% HCl and ethanol in succession to remove chemical residues. The washed GO was sonicated to get a well dispersed GO solution. At the last, any unexfoliated graphite residues were removed by another round of centrifuge. The as-made GO stock solution was stored in a cool dark place for future usage.

3.3 GO Membrane Fabrication

We synthesized a laminal GO-enabled membrane using hydrate silica gel as the cross-linker. The schematic structure of the GO membrane and the reaction mechanism are illustrated in Figure 3.1.
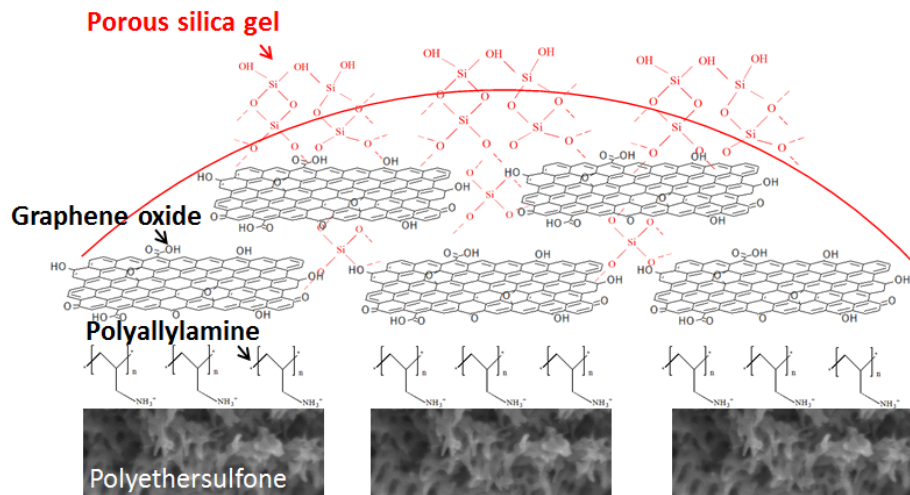
Figure 3.1 Schematic demonstration of GO membrane structure

To begin with, we rinsed the as-purchased PES membrane support with DI water to remove the potential contaminates during the packing and transportation. 1g/L of PAH solution was made with a pH of 4. We then soaked the PES membrane support in the PAH solution while having a gentle shaking. After 30 min, the membrane support was taken out and rinsed fairly with DI water.

A GO solution with pH adjusted to 3 by adding negligible amount of 30% HCl solution was sonicated first. We deposited the laminal GO layers on top of the PES membrane support by simply filtrating the GO solution through the membrane via vacuum filtration. The GO layers were subsequently soaked in a saturated sodium metasilicate solution (38 wt. %) for cross-linking and stabilization. As a final step, we rinsed the GO membrane with DI to fully remove the exceeded silicate solution and transferred the membrane into a 10% H_2SO_4 solution for further stabilization. The as-fabricated GO membranes were stored in DI water at room temperature.

3.4 Characterization Techniques

The physiochemical properties of GO nanosheets and GO membranes were characterized by Fourier transform infrared (FTIR) spectroscopy (Nicolet 6700, Thermo Scientific, Marietta, OH), scanning electron microscopy (SEM) (SU-70, Hitachi High Technologies America, Gaithersburg, MD), Transmission electron microscopy (TEM) (JEOL JEM 2100 LaB$_6$, JEOL, Peabody, MA), X-ray photoelectron spectroscopy (XPS) (Kratos AXIS 165, Kratos Analytical, UK), and zeta-potential analyzer (Zetasizer Nano ZS90, Malvern Instruments, UK).

3.4.1 SEM Sample Preparation

The PES membrane support and GO membranes with different GO loadings were dried in a 60°C oven for 12h. For cross-sectional imaging, the dried membrane samples were soaked in the liquid nitrogen to crack the membranes while maintaining a good cross-sectional structure without curvature. The membrane samples were attached to a stainless steel platform by conductive carbon taps. To enhance the conductivity of the membrane samples, a thin layer of Au particles was deposited on the membrane surface.

3.4.2 TEM Sample Preparation

The TEM samples of GO nanosheets were prepared by dropping a few diluted GO suspensions onto a lacey carbon TEM grid (TED PELLA, INC.) and dried in a 60°C oven for 8h. The samples of silane cross-linked GO nanosheets were made in a

relevantly similar way with GO membrane fabrication. Generally, a diluted GO solution with pH adjusted to 3 was dropped onto a lacy carbon TEM grid. After drying using nitrogen gas flow, we dropped a diluted sodium silicate solution on the grid. The samples were finally dried in a 60°C oven for 8h.

3.4.3 Zeta-potential Experiment

The charge property of GO solution (1g/L) was measured at different pHs. The pHs of GO suspension were adjusted by adding HCl and NH_4OH. The added amount was negligible comparing to the sample volume.

3.5 Membrane Performance Test

3.5.1 Permeability and Rejection Test

The water permeability as well as the rejection of different uncharged organic molecules and ionic species was tested in a dead-end filtration system. The overall configuration of the system is demonstrated in Figure 3.2. The filtration system was pressurized by nitrogen gas. Membranes were mounted at the bottom of an ultrafiltration cell (EMD Millipore Amicon™), which was connected to a pressure-retained feed tank. The pressure driven flow was consequently pushed through the membranes with a gentle stirring to minimize the external concentration polarization effect. The mass change of the permeat per unit time was automatically recorded by a digital balance (Denver Instruments, Denver, CO) and transferred to a PC using data acquisition software. To eliminate the compaction effects, membranes were

21

pressurized under a trans-membrane pressure of 50 psi (0.34 Mpa) for 24h before each test.
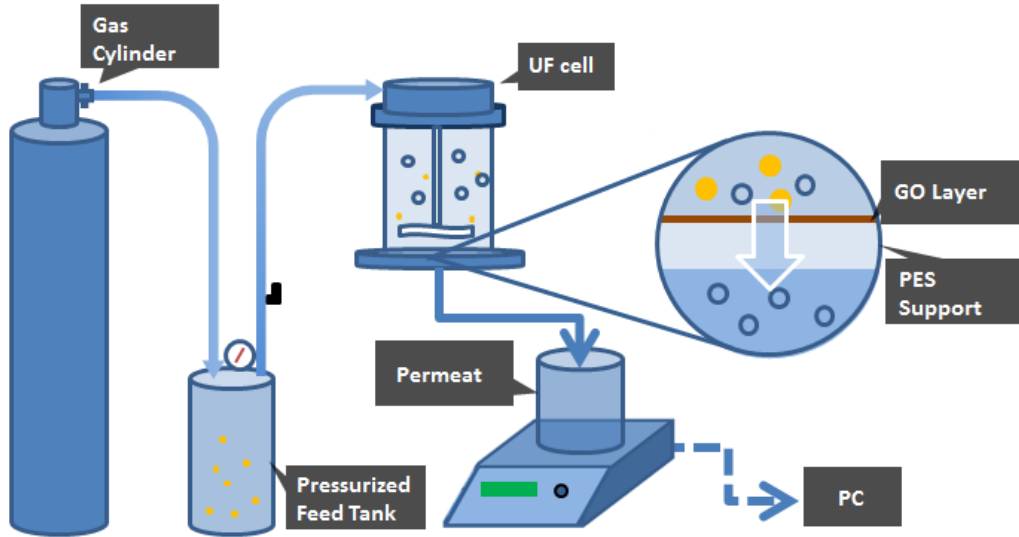
Figure 3.2 Schematic demonstration of pressurized filtration system

The permeability and rejection tests were conducted afterwards under a trans-membrane pressure of 20 psi (0.13 Mpa). Due to the fact that the ionic strength would greatly affect the aggregation tendency of GO nanosheets, and consequently determine the swelling percentage of the GO layers, we purposely equaled the ionic strength of the testing solutions according to the ideal ionic strength equation:

$$I = \frac{1}{2}\sum_i z_i^2 c_i \qquad (2)$$

Where I is the ionic strength,

z_i is the charge of ion,

c_i is the molar concentration of the ion.

For the uncharged organic molecules (e.g. glucose, sucrose, and PEG) used in the rejection test, we controlled the concentration in the same magnitude as that of the ionic species (Table 2). The viscosity of the testing solution was controlled in a reasonable rage.

For each rejection test, membranes were firstly stabilized in the system by running for 2h to reach the adsorption capacity of GO layers and PES support. Both feed and permeat samples were collected to determine the rejection percentage. For ionic species, concentration of the samples were evaluated by measuring the conductivity (Accumet Excel XL30, Thermo Scientific , Marietta, OH). The concentration of the uncharged organic molecules was evaluated by a total organic carbon analyzer (TOC-5000, Shimadzu, Columbia, MD). For each test, triplicate experiments were conducted.

Table 3.2 Rejection test solution concentration

Testing solute	Concentration/mM
Trisodium Citrate Dihydrate (TSC)	20
Sodium Sulfate (Na_2SO_4)	40
Magnesium Chloride ($MgCl_2$)	40
Sodium Chloride (NaCl)	120
Succrose	100
Glucose	100
PEG	100

3.5.2 Forward Osmosis Performance Test

A schematic illustration of the lab-scaled FO system configuration is shown in Figure 3.3. The membrane coupons with an effective area of 20 cm^2 were clamped between the feed channel and the draw channel by two seal rings in a transparent membrane cell. The flow direction of the feed solution and the draw solution were the same. We used 2 L of DI water as the feed solution for each test. The draw solutions used in this study and their concentration were listed in Table 3.3. The osmotic pressure generated by each draw solution was purposely set to equal (360psi) according to the van't Hoff equation (Equation 1). Both of the feed and draw solutions were recirculated between the cell's channels and the solution tanks. The circulated flow rate was maintained at 8.75 cm s^{-1} by two magnetic pumps. The operational temperature was maintained by a digital recirculating bath (Neslab, Newington, NH) at 25 °C. We tested the membranes performance using each of the listed draw solutions in both FO mode (with GO layers facing the feed solution) and PRO (with GO layers facing the draw solution).
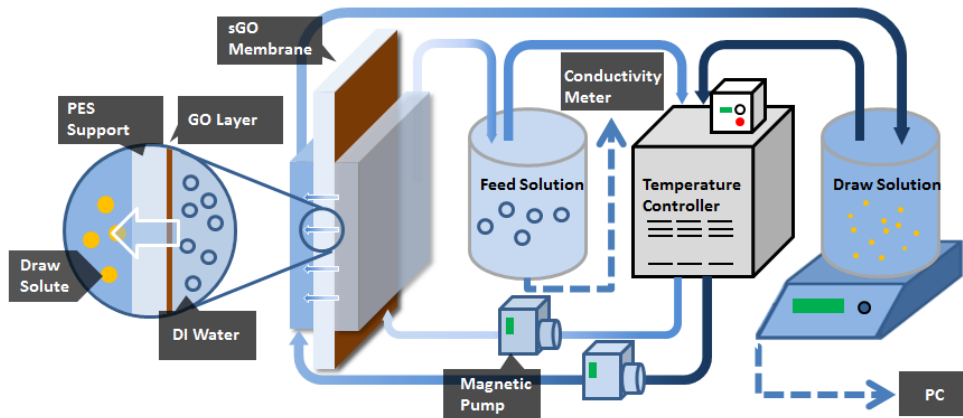
Figure 3.3 Lab-scaled forward osmosis system configuration

Table 3.3 Draw solute and their concentration for forward osmosis

Draw solute	Concentration/M
Trisodium Citrate Dihydrate (TSC)	0.25
Sodium Sulfate (Na_2SO_4)	0.33
Magnesium Chloride ($MgCl_2$)	0.33
Sodium Chloride (NaCl)	0.50

Water flux was evaluated by monitoring the mass increase in the draw solution tank with a digital balance. For the ionic species, back solute flux was analyzed by measuring the conductive in the feed solution tank with moderate stirring. For sucrose, water samples in the feed solution were collected and analyzed in a TOC analyzer. The solute flux J_s is calculated as

$$J_s = [C(V_0 - J_w At) - C_0 V_0]/At \tag{3}$$

Where, J_w is the water flux,

C_0 is the initial concentration,

V_0 is the initial volume feed solution,

t is the time, and

A is the effective membrane area (20 cm^2).

Before collecting performance data, the FO system was stabled under operation condition for 30 min. After each round of test, the membranes were stored in DI water to dissolve out the testing solutes.

3.5.3 Aging Effect Test

We investigated the GO membranes FO performance after aging for different period of time. GO membranes were aged in DI water bath open to the air at 60℃ for 12 h, 24 h, 36 h, and 48 h. We used DI water as the feed solution and 0.25 M of TSC as the draw solution. Water flux and back solute flux in FO mode and PRO mode were measured.

3.5.4 Calcification Effect Test

GO membranes were firstly tested in FO mode using DI as the feed solution and 0.25 M of TSC as the draw solution to setup a baseline. During the calcification test, 1109.8 mg of $CaCl_2$ (5 mM) was added in the feed solution, while the draw solution remained the same. The Ca^{2+} contained feed solution was subsequently recirculating on the GO membrane surface. Water flux and solute flux were measured for 12 h to compare with the previous baseline.

Chapter 4: Results and Discussion

4.1 Physicochemical Properties of GO Nanosheets

We investigated the physicochemical properties of GO by several characterization techniques as these properties could affect the subsequent GO membrane fabrication and their performance. Distinguished from its precursor graphite, the as-made GO aqueous suspension had a light brownish color due to the addition of oxygenated function groups on the carbon lattice. The initial pH of the GO suspension was measured to be around 4 and would remain stable for a long period of time. Because of the charge repulsion between the negatively charged GO nanosheets, the suspension would remain dispersed at its initial pH. In fact, the GO suspension showed no sign of aggregation and precipitation even when stored for several months. However, the charge screening effect is highly pH dependent. Figure 4.1 demonstrated the zeta-potential of the GO nanosheet in function of pHs.
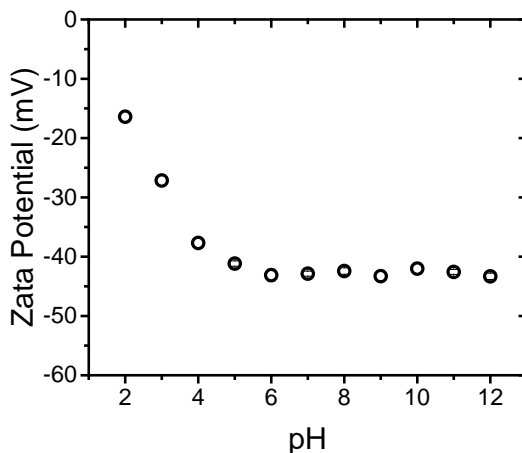
Figure 4.1 Zeta potential of GO nanosheets as a function of pH

The TEM image (Figure 4.2 (a)) shows the geometry of GO nanosheets. Typically, GO nanosheets are in the size of around 1µm with defects of several to 20 nm in diameters, which are caused by the chemical exfoliation. Figure 4.2 (b) shows the surface morphology of GO nanosheets in a higher magnification. At this point, the inoxidized graphitic region can be observed with clear repeated pattern corresponding to the sp2 aromatic carbon lattice. The darker and blurred areas could be resulting from the sp3 oxidized structures.
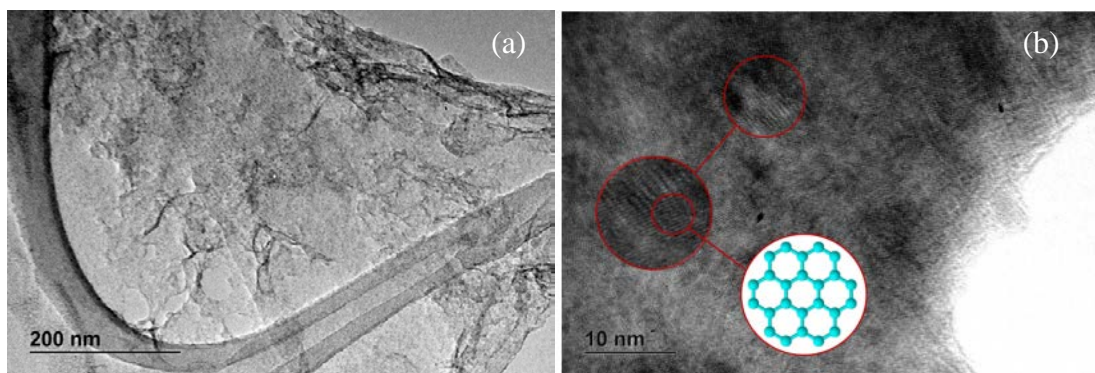
Figure 4.2 TEM image of (a) GO nanosheet, and (b) surface morphology of GO nanosheet

A further test was conducted to identify the crystallinity of GO nanosheets using the selected area (electron) diffraction (SAD) (Figure 4.3 (a)). The SAD on the pure carbon film was also analyzed as a comparative control (Figure 4.3 (b)). Generally, the bright dots-formed circle suggests a relevantly weak crystallinity resulting from the graphitic carbon lattice. The continuous bright circle represents an amorphous region, which is due to the distortion of the readily oxidized carbon lattice.
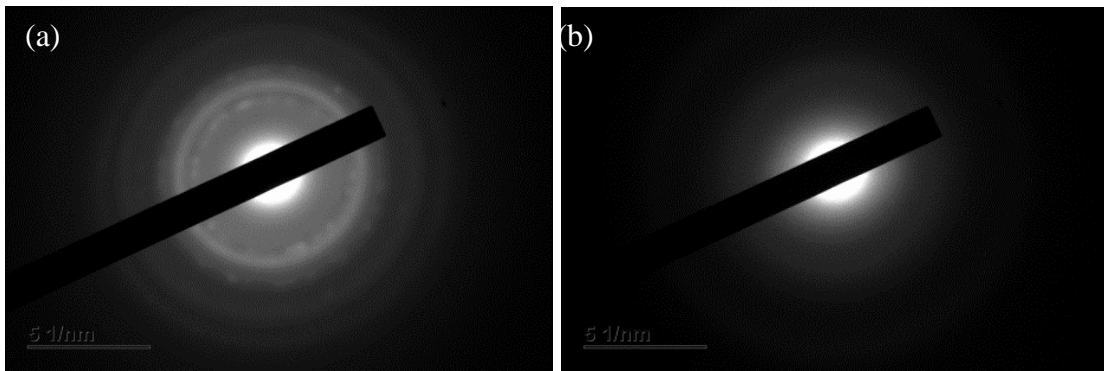
Figure 4.3 SAD patterns of (a) GO nanosheet, and (b) lacy carbon film.

The Energy-dispersive X-ray spectroscopy (EDS) (Figure 4.4) shows the quantitative signals of different elements. The detected strong Cu signals come from the cooper grids, the Cl signals are mainly due to the HCl that used for pH adjustion, and the C and O signals come from the GO nanosheets. The EDS also provides a carbon and oxygen ratio using Cliff Lorimer method (Table 4.1), which is in consistence with the previous reports[73, 74, 93].
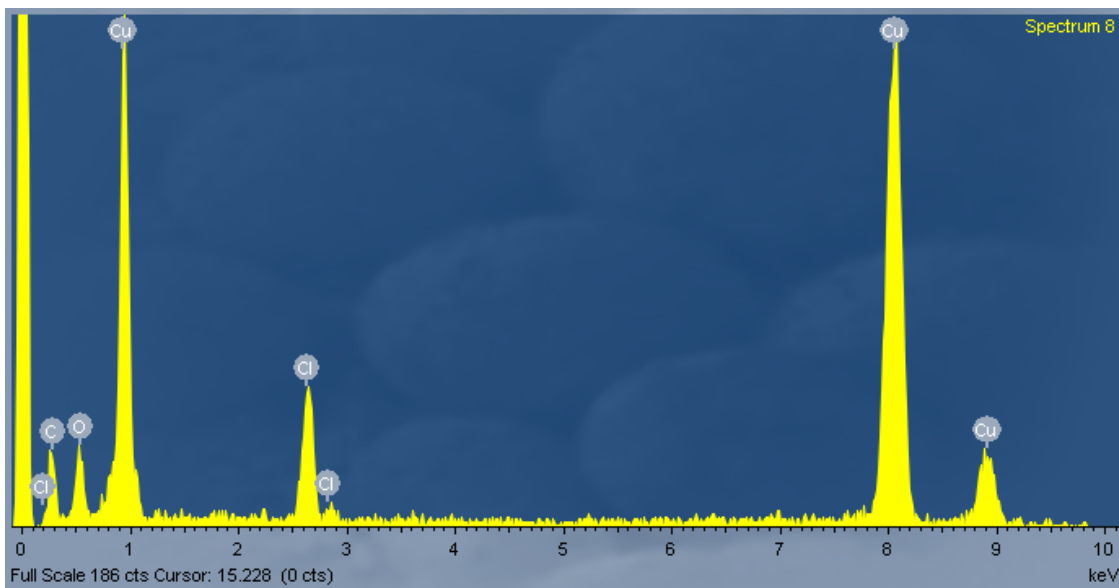
Figure 4.4 EDS spectra of GO nanosheet

Table 4.1 Quantitative analysis of C/O ratio for GO nanosheet

Element	Weight%	Atomic%
C	53.64	60.65
O	46.36	39.35
Totals	100.00	

4.2 GO Membrane Synthesis

Generally, the GO membrane has a porous support layer and a thin GO layer. The commercialized PES membrane was selected as the support layer to enhance the membrane mechanical strength. Figure 4.5 (a) shows that the PSE membrane support is relevantly thick (~120µm), which has an asymmetric structure with a porous back side (average pore size of 500 nm) (Figure 4.5 (b)), and a denser front side (average pore size of 300nm) (Figure 4.5 (c)). Such dense skin layer is considered ideal for a uniform deposition of GO layers.
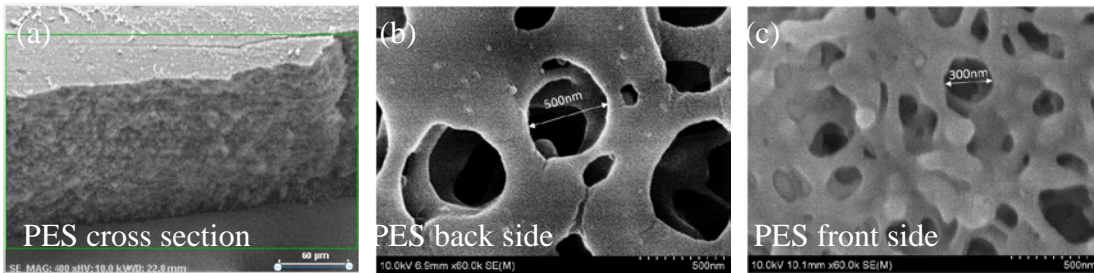
Figure 4.5 SEM image of PES membrane support from (a) the front side, (b) the back side, and (c) the cross section.

The as-purchased PES membrane surface is negatively charged due to the sulfonated functional groups. In order to create a charge-favorable media for GO

nanosheets deposition, the PES membrane supports were pretreated with the positively charged PAH. Consequently, PAH was bonded to the PES membrane surface by electrostatic interaction.

The laminal GO layers with different thickness were deposited on the PES supports by vacuum-assisted filtration. We purposely controled the GO deposition amount to manipulate the GO layer thickness. As shown in Figure 4.6, the 1mL, 2mL, and 5mL GO suspension loading resulted in the layer thickness of 70nm, 130nm, and 460nm, respectively. The strong linear relationship evidenced that the GO nanosheets have paralleled stacking feature, which enables the unique nanochannels between GO layers.
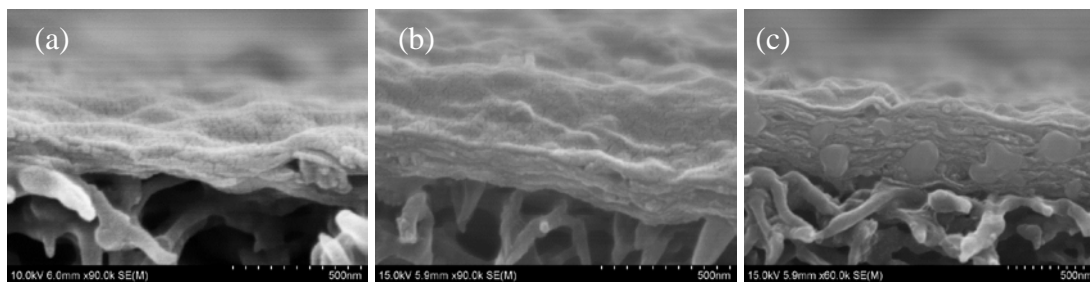
Figure 4.6 SEM images of GO membranes with (a) 1mL GO loading, (b) 2mL GO loading, and (c) 5mL GO loading.

The GO films were immediately soaked in a saturated sodium metasilicate solution for cross-linking after the filtration process. Since the GO film was not completely dried, an acidic aqueous environment (pH~3) still existed in the GO nanochannels, where an instantaneous gelation process went on forming a silica hydrogel network. The illustration of the reaction is shown in Figure 4.7 (a). This step was critical because the GO nanosheet was highly unstable and tended to re-suspend

into an aqueous solution due to its extreme hydrophilicity. The resulting silica hydrogel in the facial layers has high permeability due to the selected pH and the reduced silicate concentration in the GO nanochannels. Therefore, further silicate diffusion would not be hindered.

The reaction between the silica hydrogel and GO nanosheets can be divided into three steps. Firstly, the saturated sodium silicate solution (pH~12) provided a basic environment. The carboxyl and hydroxyl contained GO nanosheets can be regarded as an organic acid or an organic alcohol, or even both in such condition. The second step involved the reaction with silica hydrogel (Figure 4.7 (b)). Briefly, the entire reaction process was a dehydration reaction. The silica hydrogel tended to lose its flowability and hence condense towards solidification when its viscosity exceeded the critical value. In a third step, the silica gel further dehydrated and became hardened.
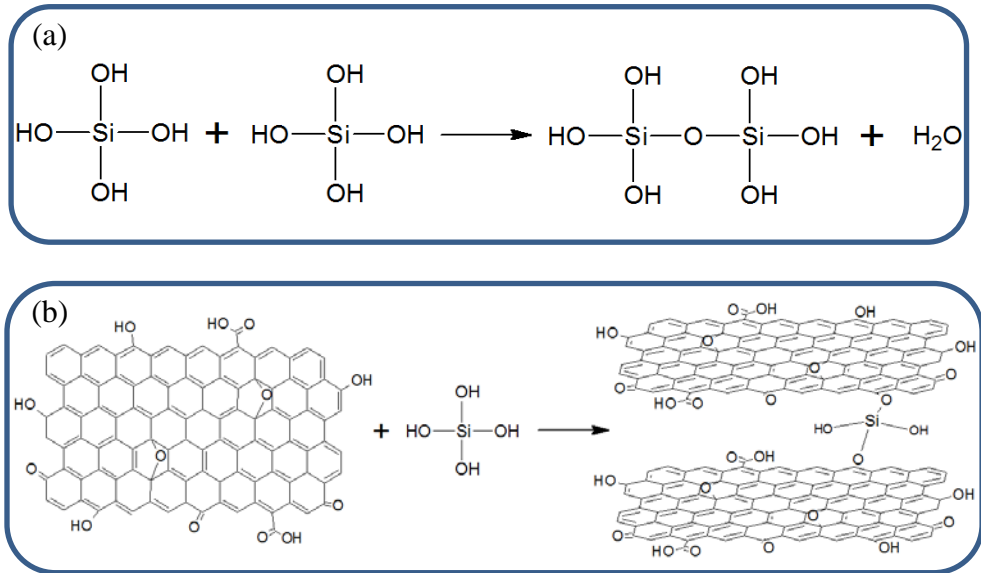
Figure 4.7 Reaction mechanism for (a) silica gelation, and (b) GO cross-linking process

After reacted in the saturated sodium silicate solution for 12 h, the GO membranes were rinsed and transferred to a 10% H_2SO_4 solution, which is a typical approach used in the sol-gel process for further stabilization.

Color of the pure GO deposited membranes varied from light yellow to dark brown depending on the different GO loading amount. A slight loss of its original color and turning towards white could be observed after the cross-linking process, which was caused by homogenous nucleation of silica gel.

4.3 GO Membrane Characterization

FTIR was used to examine the membrane functional groups, as well as their changes after each synthesis steps. As shown in Figure 4.8 , a slight peak change at 1670 cm^{-1} can be found for primary amines after PAH treatment, which confirms the successful PAH deposition on the membrane surface. The relevantly subtle change could be due to the signal interference from the C=C stretching.
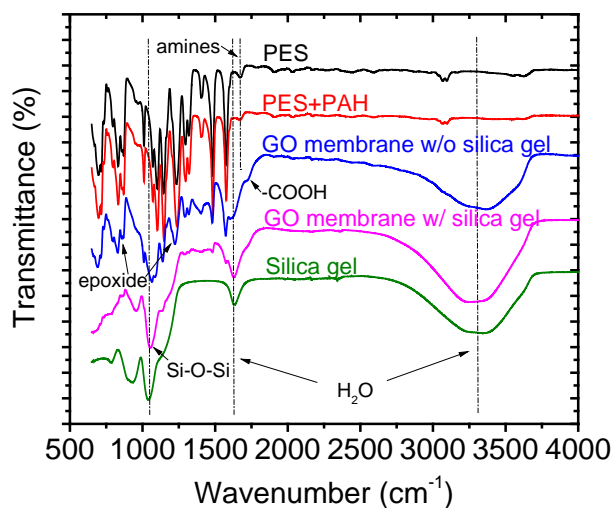
Figure 4.8 FTIR spectra of different membrane fabrication steps

The FTIR spectra of the 2mL GO deposited membranes (blue curve) shows featured peaks at 1710 cm^{-1} for carboxyl groups, peaks at 856 cm^{-1} and 1223 cm^{-1} for epoxide groups. However, since the GO films were only 150 nm thick, the infrared can easily penetrate the GO layers and detect functional groups of the PES supports, which explains the similar peaks observed from both PES supports and GO membranes without silica gel.

The FTIR spectra of the silane cross-linked 2mL GO deposited membranes (purple curve) has a strong peak for the covalent bonding between Si and O at 1053 cm^{-1}, which is absent from the spectra of the uncross-linked GO membranes. Compared to the spectra of pure silica gel (green curve), the similar peaks were found indicating the existence of silica gel in the GO layers. Additionally, the peaks for carboxyl and epoxide groups were diminished significantly after the cross-linking, which lead to an assumption that both oxygenated functional groups participated in the reaction with silica gel. However, since the IR signals can be easily interfered and even blocked by the additional mass deposition, whether the previous speculation was valid remains unclear at this stage.

XPS spectra were also applied to differentiate the chemical composition of GO membranes before and after the silane cross-linking process (Figure 4.9). An enhanced emission peak for O1s at 532.7 eV and a reduced peak for C1s at 284.6 eV were observed after the silane cross-linking, revealing a major C/O ratio change caused by the introduced Si-O cross-linkers. Two emission peaks for Si2p at 102.9 eV and Si2s at 153.3 eV, again confirmed the existence of silicon in the GO membranes.
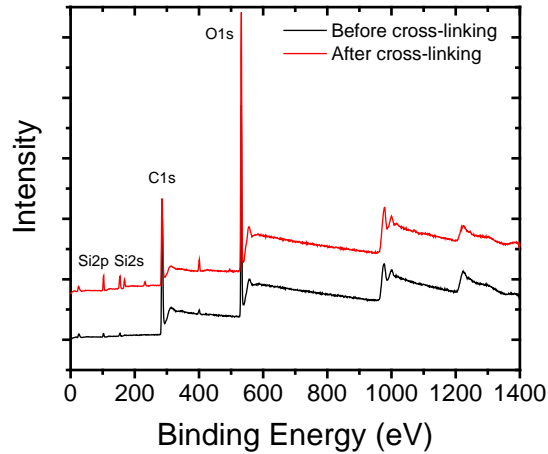
Figure 4.9 XPS spectra of GO membranes before and after silane cross-linking

We resolved the C1s spectra into three peaks (Figure 4.10), which are C-C (C-H), C-OH (C-O-C), and HO-C=O with corresponding binding energy of 284.3 eV, 286.4 eV, and 288.1 eV respectively. Since the cross-linking reaction did not involve the carbon lattice, the absolute amount of C-C/C-H should remain the same after cross-linking. Moreover, we found that the component ration between C-C/C-H and C-OH also remain relatively constant. At the time a significant intensity decrease for COOH emission peak was found after the cross-linking process.
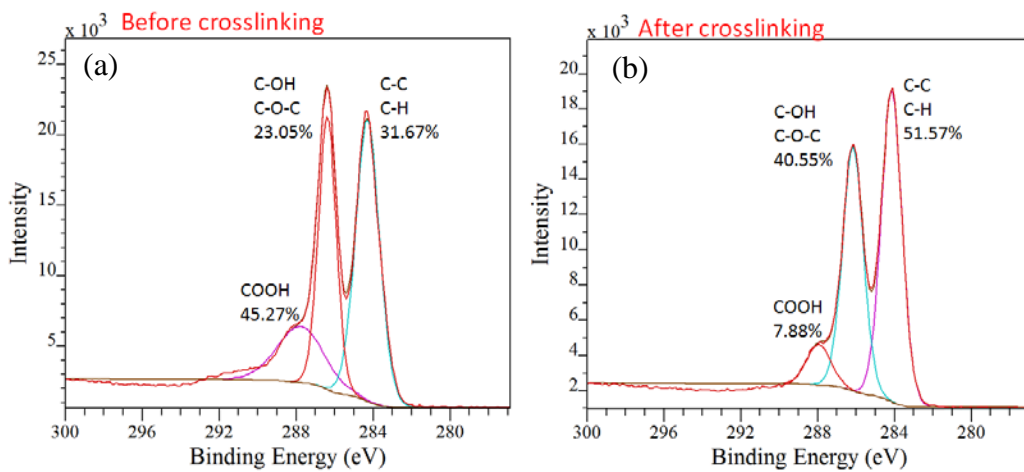
Figure 4.10 XPS spectra of C1s for (a) GO membrane without silane cross-linking, and (b) GO membrane with silane cross-linking

To identify which oxygenated functional group was the major one contributed to the cross-linking O1s spectra was also investigated. As shown in Figure 4.11, the emission peak of the overall O1s increased and shifted slightly from 532.3 eV to 531.9 eV after cross-linking due to the addition of a strong featured peak of Si-O-Si at 531.4 eV. A significant decrease of carboxyl and carbonyl groups was observed indicating that the cross-linking reaction was mainly between the silica gel and these two functional groups. Slight peak decrease for epoxide and hydroxyl (C-OH) groups also suggested that both of them contributed in the cross-linking with silica gel yet to a less extent. An emission peak corresponding to SiO2 was found after cross-linking, which could result from the complete dehydration of silica gel. The XPS results were in consistence with the mentioned reaction mechanism between GO and silica gel.
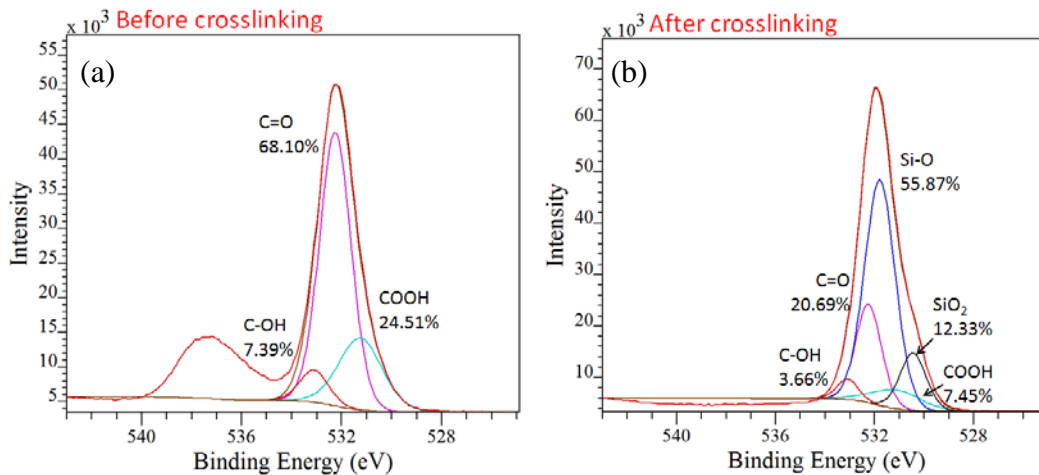
Figure 4.11 XPS spectra of O1s for (a) GO membrane without silane cross-linking, and (b) GO membrane with silane cross-linking

4.4 GO Membrane Permeability and Selectivity

Water permeability of the synthesized GO membrane was test under a trans-membrane pressure of 20 psi (0.16 MPa). The results (Figure 4.12 (a)) show that with

the deposition of 1mL to 5mL GO suspension, the water flux of PES membranes dropped from 942 ± 21.6 l/m^2-h to $8 - 42$ l/m^2-h. Moreover, the water flux shows a linear decrease as the GO layers get thicker. A possible explanation is the overall tortuosity of the GO membrane increases greatly because of the thicker laminal GO layers. In addition, the defects on the GO nanosheets which are the potential water pathway in the thinner GO film are most likely to be covered when more GO were deposited.
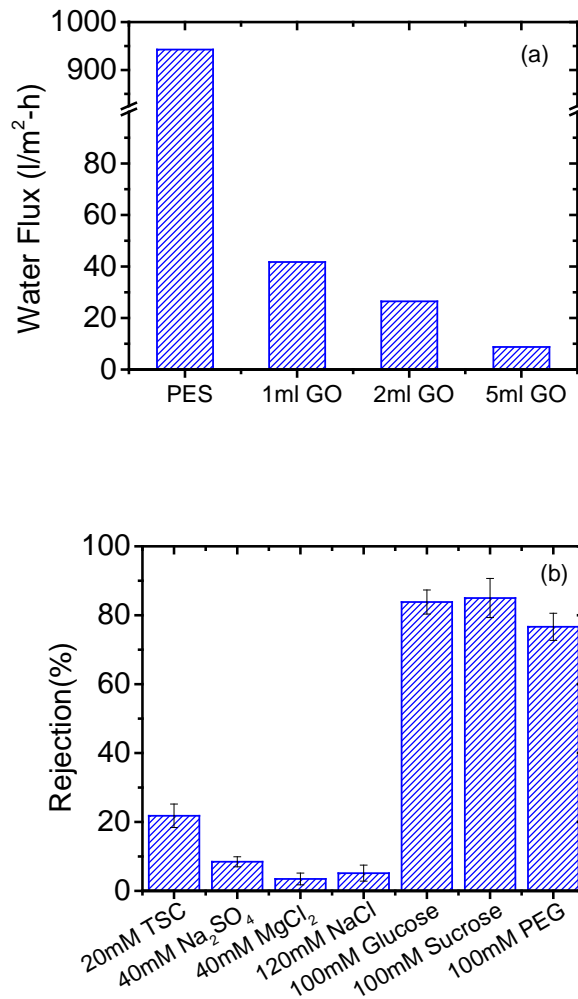
Figure 4.12 GO membrane (a) pure water permeability as a function of GO loading, and (b) rejection of different solutes.

Furthermore, the increase in the total GO film thickness can also result in a higher silane cross-linker amount. At this stage, we suspect that the silica gel network may cause some friction of the water flow and hence increase the water resistance. Yet, this speculation needs to be proved by studies in the future.

The rejection tests of the silane cross-linked GO membrane were also conducted under a trans-membrane pressure of 20 psi. Unique selectivity can be observed in the rejection results (Figure 4.12 (b)). For all the ionic species, despite of the charge and molecular size difference, the rejections were relevantly low (5%~25%), indicating that the synthesized GO membranes may not be efficient in terms of removing dissolved salts. The higher rejection of the negatively charged divalent and trivalent ionic species (i.e. TSC and Na_2SO_4) and lower rejection of the positively charged divalent ion ($MgCl_2$) reveal the fact that the main rejection mechanism was due to the charge repulsion caused by the negatively charge GO layers.

Nevertheless, the GO membrane rejection of the uncharged organic molecules remained at a high level (75% ~ 85%). This unique rejection property was just opposite to the traditional polymeric membranes. Normally, the polymeric membranes are more capable of rejecting ionic species due to the surface charge effect. The GO deposition, though charge effects still exist, has entirely changed the selectivity of the membrane.

Two reasonable hypotheses were made at this point. The GO layers, though were stabilized by the silica gel, still swelled in the ionic solutions due to the elastic structure of silane cross-linkers, which explains low rejection of the ionic species. Yet, when tested with the uncharged organic molecules, the GO layers remained

38

tight. The second hypothesis was that rather than the swelling issue, the GO layers have unique interactions with the organic molecules resulting in a hindered diffusion. To extrapolate the unique rejection phenomena, we retested the GO membrane rejection of the uncharged organic molecules with the presence of 20mM of NaCl. The results are showed in Figure 4.13. A significant decrease in PEG rejection was found after blending in the ionic species, which is an implication that the GO layers swelled in an ionic solution. However, only slight decrease can be found in glucose and sucrose rejection. We tried to explain the differences in rejection by looking at the molecular structure of the three selected organics. Glucose is basically the monomer of sucrose. Both of them have many hydroxyl groups on the edges, which form the electron donor and acceptor complex with the carbonyl groups on GO surface. On the other hand, PEG, although has a much higher molecular weight, is composited by a long carbon chain which only has von der waals interaction with the GO nanosheet. Therefore, the hindered diffusion of PEG was mainly due to the size exclusion, which would be highly affected by the width of GO nanochannels.

In summary, the testing results proved the swelling facts of GO layers in ionic environment. Uncharged organic molecules with the aromatic carbon structure have a hindered diffusion in the GO nanochannels, while the rejection of ionic species is independent with the hindered diffusion of organic molecules.

According to the unique rejection properties, the synthesized GO membranes possess high separation capability to remove the aromatic organics from the ionic solution or vice versa.
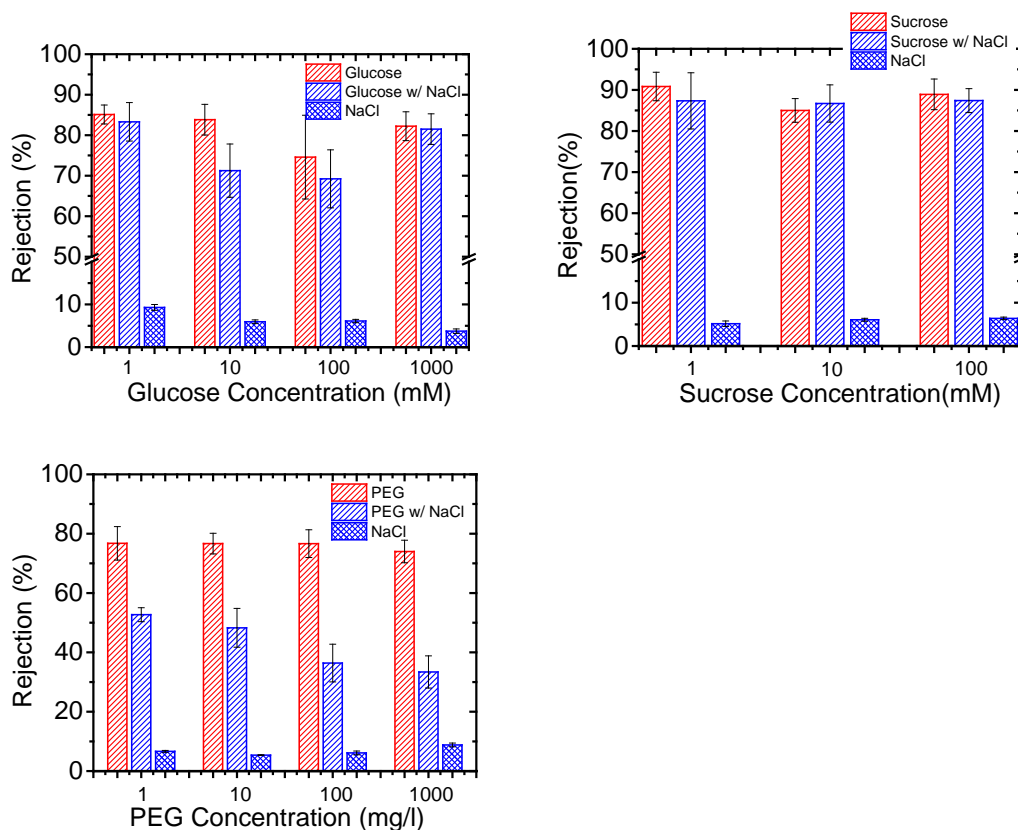
Figure 4.13 GO membrane rejection of the uncharged organic molecules.

4.5 GO Membrane Performance in Forward Osmosis

The water flux and back solute flux of the GO membranes with different GO deposition amount were measured in a forward osmosis system, in which DI water was used as feed solution and 0.25 M TSC was used as draw solution. The commercialized cellulose triacetate (CTA) membrane was tested with the same experimental condition as a control. Figure 4.14 (a) shows a high water flux ($\sim$35 l/m^2-h) for the 1mL GO deposited membrane and an even higher water flux ($\sim$39 l/m^2-h) for the 2 mL GO deposition in the FO mode. Unlike the results in the pressurized system, the doubled GO loading did not lower water flux due to the

intrinsic difference between the hydraulic pressure and the osmotic pressure. The 1 mL GO deposited membrane due to its ultrathin GO coverage was considered to have imperfections on the GO layers. The existence of large pores can greatly increase the water permeability in the pressurized system, however, would cause the loss of osmotic pressure in the forward osmosis system. The further deposition of GO layers (5 mL GO) shows a significant decrease in water flux mainly because of the low permeability of the membrane.
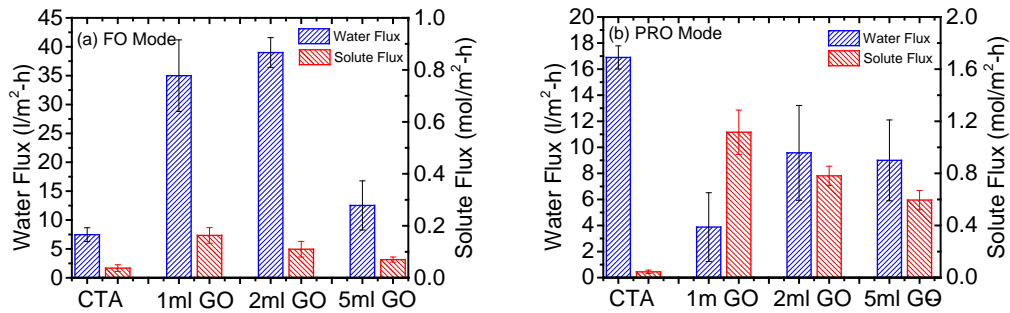
Figure 4.14 Water flux and back solute flux as a function of GO loading in (a) FO mode, and (b) PRO mode

To understand the solute transport in the GO layers, the back solute flux was measured as well. A slight decreasing trend was observed with the increasing of GO layers, which was in consistence with the previous theory. The higher GO deposition would lower the chance that any large pores are left behind and higher the solute retention capacity due to the higher GO film thickness. Compared to the CTA membrane, the synthesized GO membranes have enhanced water flux (6~7 folders) and comparable back solute flux.

Nevertheless, relevantly low water flux and high solute flux was observed in PRO mode (Figure 4.14 (b)). Normally, membranes (e.g. CTA and TFC membranes) have

higher water in PRO mode than FO mode because of the reduced internal concentration polarization (ICP) effect. We suspected that the swelling issue also affected the membrane performance in the forward osmosis system. In the PRO mode, the GO layers directly contact with the high ionic strength solution resulting in an evitable swelling of GO layers. As the interlayer spacing getting larger, the membrane lost its selectivity and osmotic driving force. Consequently, more solute can pass through the membrane causing the concentration gradient drop in the bulk solution. On contrary, in FO mode, because of the significant ICP effect, the real solute concentration in the GO layers could be much lower than that in the draw solution resulting in a minimized swelling issue.

We also tested the water flux and back solute flux of the synthesized GO membranes in FO and PRO mode using different ionic species as the draw solute. Figure 4.15 (a) shows that in FO mode, GO membranes have high water flux and relatively low back solute flux when using the negatively charged divalent and trivalent ions (TSC and Na_2SO_4) as the draw solute. On the contrary, extremely low water flux and high solute flux were observed when using monovalent ion (NaCl) and positively charged divalent ion ($MgCl_2$), which again proved that the hindered diffusion in GO layers was dominated by charge repulsion.

In PRO mode (Figure 4.15 (b)), though swelling issues were found in every testing condition, the monovalent ion and positively charged divalent ion seems to have a more significant impact on the GO swelling. A reasonable assumption is that the charge repulsion effect prevented the GO swelling though only to small extent.
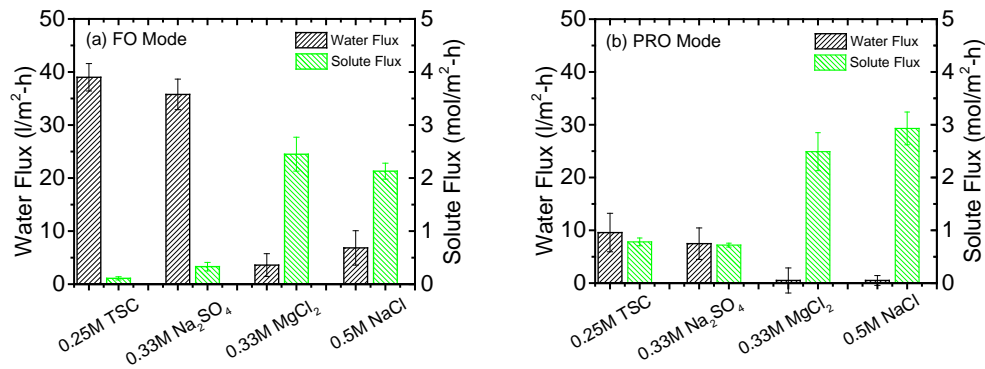
Figure 4.15 Water flux and solute flux of GO membranes with different ionic species as draw solute in (a) FO mode, and (b) PRO mode

To summarize, the synthesized GO membrane demonstrates higher water flux and lower solute flux with multivalent anions as draw solutes than with monovalent salts or multivalent cations in FO mode. In PRO mode, because of the swelling effect caused by the high ionic strength environment, the GO membrane reacted like an "open gate" that allows the passage of both water molecules and ions. The unique directional flow could have some potential applications in the smart membrane systems.

4.6 Membrane Stability Evaluation

Apart from the interests in GO membrane performance, a major concern is the stability of the membrane in a long period of running. Herein, we investigated the aging effect and calcification effect on the GO membrane performance in the FO system.

4.6.1 Aging Effect Evaluation

A major concern for using silica gel as the cross-linker is the potential aging effects. The aging process is basically the gradual dehydration of silica gel. As more and more water molecules are excluded from the silica structure, the silica gel loses its elasticity and becomes stronger with the time. Finally, the silica gel could form highly condensed $(SiO_2)_n$ structure, which could greatly lower the membrane permeability. Thus, we found it valuable to understand the aging effects on the membrane performance.

As shown in Figure 4.16, the water flux remained ralevently stable in both FO and PRO mode over the aging process. The water flux decreased for only 2.36% in FO
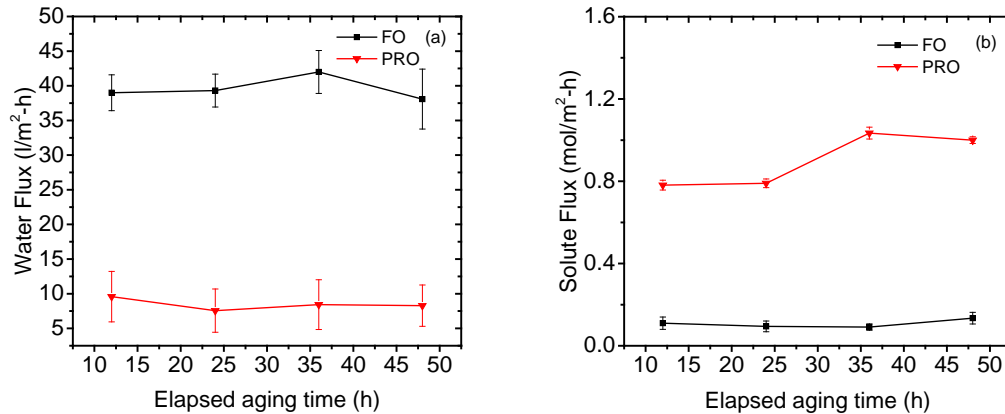
Figure 4.16 Membrane performance after aging: (a) water flux, and (b) solute flux, 0.25 M TSC was used as draw solution

mode and 13.5% in PRO mode after 48 h of aging. Note that, the aging process was accelarated by increasing the environment tempreture, so the limited aging time can represent a long period of aging time in the real operational condition. The solute flux increased slightly (21.8% in FO mode and 28% in PRO mode), which can be

explained by the decrease in charge repulsion effect as hard silica scaling forming on GO surface.

4.6.2 Calcification Effect Evaluation

Silica gel is known for its chemical inertness, which is desirable for making a more chemically stable membrane. However, the positively charged Ca^{2+} ions can be attracted to the negatively charged silica gel matrix and subsequently convert into hard calcium silicate hydrate (C-S-H). The reaction can be schematically represented as following:

$$Ca^{2+} + H_2SiO_4^{2-} + 2H_2O \rightarrow CaSiO_4 \cdot 2H_2O$$
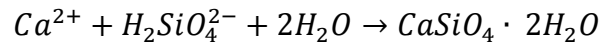
The deposition of calcium silicate hydrate can greatly change the roughness of GO layers and eventually affect the membrane performance.

In a FO system, we monitored the water flux trend of an as-synthesized GO membrane as a baseline and evaluated the calcification effect by purposely adding $CaCl_2$ in the feed solution afterwards. As shown in Figure 4.17, water flux for both tests has a gradual decline over the time due to the dilution effect in the draw solution. Compared to the baseline, membrane with Ca^{2+} ions dosage had less water flux decrease over the time and maintained a higher water flux ($\sim$ 10.1%) after 12 h. The observation suggests the possibility that the deposition of Ca^{2+} ions on the membrane surface can help form a tighter membrane surface. This assumption is in consistence with the slightly reduced back solute flux.
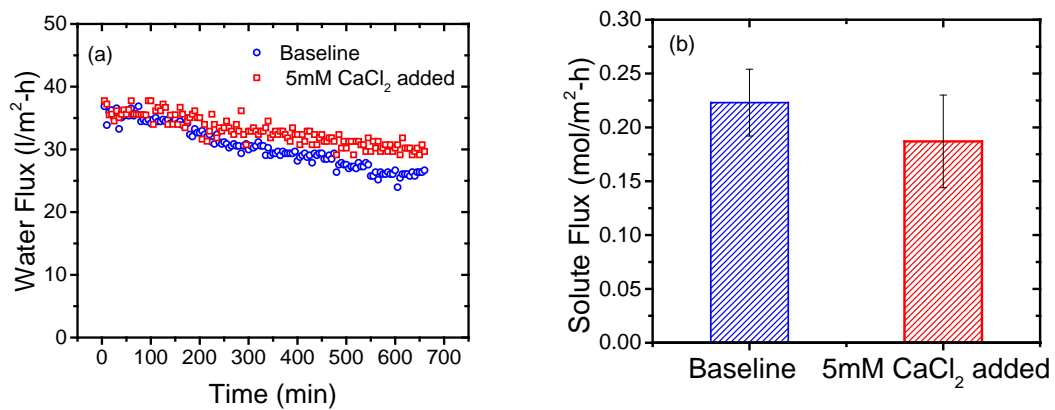
Figure 4.17 GO membrane (a) water flux, and (b) solute flux over time with the calcification effects

Chapter 5: Conclusions

5.1 Fulfillment of Research Objectives

The ultimate goal of this research is to synthesis a stable GO-enabled membrane which could potentially be used for water purification and to understand the water and solute transport mechanisms in GO layers. Toward this goal, this study aims to develop a silane cross-linked GO membrane, which demonstrates unique transport phenomena in pressurized filtration and forward osmosis. The silica gel is proved to be an efficient inorganic cross-linker for GO membrane stabilization. Characterization on both GO nanosheet and the subsequently synthesized GO membrane help understand the physiochemical properties and structure of the GO selective layers. The membrane performance experiments provide insight on transport mechanisms by demonstrating high selectivity (high rejection of the uncharged organic molecules and low rejection of ionic species) and some unique Janus effects in forward osmosis (allowing the permeation of ions on one direction while blocking the permeation on the other direction). More specifically, the following objectives of the study have been achieved through this research:

1. Developing a simple synthesis approach to make cross-linked GO membranes using silica gel as a cross-linker;

2. Understanding the physiochemical properties of GO nanosheets as well as the synthesized GO membrane using characterization techniques such as FTIR, SEM, TEM, EDS, SAD, XPS;

3. Evaluating the performance of GO membrane in both pressurized filtration and forward osmosis membrane systems under different experimental conditions;

4. Investigating the stability of GO membrane over a long time of aging and calcification; and

5. Fundamentally understanding the transport mechanisms controlling membrane performance.

5.2 Summary of Conclusions

The following conclusions can be reached from this study:

1. Silica gel can effectively cross-link GO layers by three reaction steps including an instantaneous gelation between GO nanosheets, a subsequent dehydration reaction with oxygenated functional groups on GO nanosheet, and finally a condensation process for further stabilization.

2. The GO membrane demonstrates high rejection of neutral organic molecules, especially those contain aromatic carbon structure, but low rejection of ionic species.

3. The GO membrane exhibits unique Janus properties and thus enabled directional flow most likely due to swelling effects in ionic solutions

4. The stability of GO membrane was confirmed by evaluating the membrane performance after long time aging and calcification treatment.

5.3 Implications for Future Study

The silane cross-linked GO membrane demonstrates unique transport phenomena. It provides a high rejection of uncharged organic molecule and low rejection of ionic species. Accordingly, this type of membrane could be used to efficiently remove uncharged organics from the water. In this case, it has wide potential applications including removal of the targeting humid acid, pesticides, nature organic molecules (NOMs), and pharmaceuticals. Moreover, due to the rejection rate difference, this type of GO membrane can also be used to separate the organic molecules and the ionic species, which cannot be easily achieved by the traditional polymeric membranes.

The Janus gating phenomena can be potentially used in a smart membrane system or some other specific applications. Generally, the GO membrane is sensitive to the environmental ionic strength. The GO layers are relevantly impermeable for the ions in a low ionic strength environment and would become permeable as the environmental ionic strength arises. Thus, the potential applications include but not limit to ionic strength sensors and drug delivery.

Since the inorganic cross-linker was found to be successful in GO membrane stabilization, future work needs to be done to further improve the membrane synthesis methods. Ideally, GO-enabled membrane could achieve ultrafast water transport while rejecting targeted solutes. Its applications in both water purification and desalination need to be further studied.

Bibliography

1.   Cath, T.Y., A.E. Childress, and M. Elimelech, *Forward osmosis: Principles, applications, and recent developments.* Journal of Membrane Science, 2006. **281**(1-2): p. 70-87.

2.   Shannon, M.A., et al., *Science and technology for water purification in the coming decades.* Nature, 2008. **452**(7185): p. 301-310.

3.   Yip, N.Y., et al., *High Performance Thin-Film Composite Forward Osmosis Membrane.* Environmental Science & Technology, 2010. **44**(10): p. 3812-3818.

4.   Logan, B.E. and M. Elimelech, *Membrane-based processes for sustainable power generation using water.* Nature, 2012. **488**(7411): p. 313-319.

5.   Shaffer, D.L., et al., *Desalination and Reuse of High-Salinity Shale Gas Produced Water: Drivers, Technologies, and Future Directions.* Environmental Science & Technology, 2013. **47**(17): p. 9569-9583.

6.   Pendergast, M.M. and E.M.V. Hoek, *A review of water treatment membrane nanotechnologies.* Energy & Environmental Science, 2011. **4**(6): p. 1946-1971.

7.   Van der Bruggen, B., et al., *A review of pressure-driven membrane processes in wastewater treatment and drinking water production.* Environmental Progress, 2003. **22**(1): p. 46-56.

8.   Escobar, I.C. and B. Van der Bruggen, *Microfiltration and Ultrafiltration Membrane Science and Technology.* Journal of Applied Polymer Science, 2015. **132**(21).

9.   Alspach, B., et al., *Microfiltration and ultrafiltration membranes for drinking water.* Journal American Water Works Association, 2008. **100**(12): p. 84-97.

10.   Castaing, J.B., et al., *Investigating submerged ultrafiltration (UF) and microfiltration (MF) membranes for seawater pre-treatment dedicated to total removal of undesirable micro-algae.* Desalination, 2010. **253**(1-3): p. 71-77.

11.   Fane, A.G., C.Y. Tang, and R. Wang, *Membrane Technology for Water: Microfiltration, Ultrafiltration, Nanofiltration, and Reverse Osmosis.* Treatise on Water Science, Vol 4: Water-Quality Engineering, 2011: p. 301-335.

12.   Gutierrez-Rivera, L.E., et al., *Characterization of the Selectivity of Microsieves Using a Cross-Flow Microfiltration System.* Brazilian Journal of Chemical Engineering, 2010. **27**(4): p. 677-685.

13.   Escoda, A., et al., *Determining the Dielectric Constant inside Pores of Nanofiltration Membranes from Membrane Potential Measurements.* Langmuir, 2010. **26**(18): p. 14628-14635.

14.   Buetehorn, S., et al., *Permeate flux decline in cross-flow microfiltration at constant pressure.* Desalination, 2010. **250**(3): p. 985-990.

15.   Chang, E.E., et al., *A simplified method for elucidating the effect of size exclusion on nanofiltration membranes.* Separation and Purification Technology, 2012. **85**: p. 1-7.

16.   Hsieh, H.P., R.R. Bhave, and H.L. Fleming, *Microporous Alumina Membranes.* Journal of Membrane Science, 1988. **39**(3): p. 221-241.

17.	Bhattacharyya, D., et al., *Membrane Ultrafiltration of a Nonionic Surfactant and Inorganic Salts from Complex Aqueous Suspensions - Design for Water Reuse.* Aiche Journal, 1975. **21**(6): p. 1057-1065.

18.	Elmaleh, S. and W. Naceur, *Transport of Water through an Inorganic Composite Membrane.* Journal of Membrane Science, 1992. **66**(2-3): p. 227-234.

19.	Bhave, R.R., *Ceramic Membrane-Based Filtration Systems for the Treatment of Process Water in the Food-Industry.* Abstracts of Papers of the American Chemical Society, 1994. **207**: p. 25-Agfd.

20.	Kolsch, P., et al., *A ceramic membrane for separation of water from organic solvents.* Chemie Ingenieur Technik, 2000. **72**(10): p. 1167-1173.

21.	Szmukata, M., et al., *Analysis of possibility of applying the pressure driven membrane process and ceramic membrane for contaminant removal from natural water.* VIII National Polish Scientific Conference on Complex and Detailed Problems of Environmental Engineering, 2007(23): p. 543-555.

22.	Cordeiro, V.V., et al., *Porous Anisotropic Alumina Ceramic Membrane: Preparation and Characterization.* Advanced Powder Technology Viii, Pts 1 and 2, 2012. **727-728**: p. 1485-1489.

23.	Ke, X.B., et al., *Integrating efficient filtration and visible-light photocatalysis by loading Ag-doped zeolite Y particles on filtration membrane of alumina nanofibers.* Journal of Membrane Science, 2011. **375**(1-2): p. 69-74.

24.	Tsuru, T., et al., *Permeation Properties of Hydrogen and Water Vapor Through Porous Silica Membranes at High Temperatures.* Aiche Journal, 2011. **57**(3): p. 618-629.

25.	Duke, M.C., et al., *Seawater desalination performance of MFI type membranes made by secondary growth.* Separation and Purification Technology, 2009. **68**(3): p. 343-350.

26.	Howe, K.J. and M.M. Clark, *Fouling of microfiltration and ultrafiltration membranes by natural waters.* Environmental Science & Technology, 2002. **36**(16): p. 3571-3576.

27.	Kumar, R. and A.F. Ismail, *Fouling control on microfiltration/ultrafiltration membranes: Effects of morphology, hydrophilicity, and charge.* Journal of Applied Polymer Science, 2015. **132**(21).

28.	Nguyen, S.T., F.A. Roddick, and J.L. Harris, *Membrane foulants and fouling mechanisms in microfiltration and ultrafiltration of an activated sludge effluent.* Water Science and Technology, 2010. **62**(9): p. 1975-1983.

29.	Bolton, G., D. LaCasse, and R. Kuriyel, *Combined models of membrane fouling: Development and application to microfiltration and ultrafiltration of biological fluids.* Journal of Membrane Science, 2006. **277**(1-2): p. 75-84.

30.	Furukawa, T., et al., *Analysis of the membrane fouling on cross-flow ultrafiltration and microfiltration of soy sauce lees.* Kagaku Kogaku Ronbunshu, 2000. **26**(3): p. 431-436.

31.	Yamamura, H., K. Kimura, and Y. Watanabe, *Mechanism involved in the evolution of physically irreversible fouling in microfiltration and ultrafiltration membranes used for drinking water treatment.* Environmental Science & Technology, 2007. **41**(19): p. 6789-6794.

32.   Hilal, N., et al., *A comprehensive review of nanofiltration membranes: Treatment, pretreatment, modelling, and atomic force microscopy.* Desalination, 2004. **170**(3): p. 281-308.

33.   Tu, S.C., et al., *Predictive membrane transport model for nanofiltration precesses in water treatment.* Aiche Journal, 2001. **47**(6): p. 1346-1362.

34.   Chaabane, T., et al., *Dynamic modeling of mass transfer through a nanofiltration membrane using calcium salt in drinking water.* Desalination, 2003. **152**(1-3): p. 275-280.

35.   Ahmad, A.L., et al., *Development of a highly hydrophilic nanofiltration membrane for desalination and water treatment.* Desalination, 2004. **168**: p. 215-221.

36.   Hu, K. and J.M. Dickson, *Nanofiltration membrane performance on fluoride removal from water.* Journal of Membrane Science, 2006. **279**(1-2): p. 529-538.

37.   Nanda, D., et al., *Effect of pH on membrane morphology, fouling potential, and filtration performance of nanofiltration membrane for water softening.* Journal of Membrane Science, 2010. **349**(1-2): p. 411-420.

38.   Dowhan, W., *Molecular basis for membrane phospholipid diversity: Why are there so many lipids?* Annual Review of Biochemistry, 1997. **66**: p. 199-232.

39.   Negaresh, E., et al., *Selective separation of contaminants from paper mill effluent using nanofiltration.* Chemical Engineering Research & Design, 2012. **90**(4): p. 576-583.

40.   Her, N., et al., *Identification of nanofiltration membrane foulants.* Water Research, 2007. **41**(17): p. 3936-3947.

41.   Nghiem, L.D., A.I. Schafer, and M. Elimelech, *Role of electrostatic interactions in the retention of pharmaceutically active contaminants by a loose nanofiltration membrane.* Journal of Membrane Science, 2006. **286**(1-2): p. 52-59.

42.   Abdessemed, D., S. Hamouni, and G. Nezzal, *State of the reverse osmosis membrane of sea water corso plant desalination (Algiers).* Proceedings of the Jmsm 2008 Conference, 2009. **2**(3): p. 1469-1474.

43.   Lee, K.P., T.C. Arnot, and D. Mattia, *A review of reverse osmosis membrane materials for desalination-Development to date and future potential.* Journal of Membrane Science, 2011. **370**(1-2): p. 1-22.

44.   Wang, J., S.Y. Lai, and Y. He, *Research on Reverse Osmosis Membrane Materials for Seawater Desalination.* Advanced Research on Environmental Science and Material Application, 2012. **600**: p. 100-103.

45.   Gullinkala, T., et al., *Desalination: Reverse Osmosis and Membrane Distillation.* Sustainable Water for the Future: Water Recycling Versus Desalination, 2010. **2**: p. 65-93.

46.   Yu, S.C., et al., *Performance enhancement in interfacially synthesized thin-film composite polyamide-urethane reverse osmosis membrane for seawater desalination.* Journal of Membrane Science, 2009. **342**(1-2): p. 313-320.

47.   Cadotte, J.E., et al., *New Thin-Film Composite Seawater Reverse-Osmosis Membrane.* Desalination, 1980. **32**(1-3): p. 25-31.

48. Riley, R.L., et al., *Recent Developments in Thin-Film Composite Reverse-Osmosis Membrane Systems.* Desalination, 1981. **36**(3): p. 207-233.

49. Liu, M.H., et al., *Preparation, structure characteristics and separation properties of thin-film composite polyamide-urethane seawater reverse osmosis membrane.* Journal of Membrane Science, 2008. **325**(2): p. 947-956.

50. Misdan, N., W.J. Lau, and A.F. Ismail, *Seawater Reverse Osmosis (SWRO) desalination by thin-film composite membrane-Current development, challenges and future prospects.* Desalination, 2012. **287**: p. 228-237.

51. Safarpour, M., A. Khataee, and V. Vatanpour, *Thin film nanocomposite reverse osmosis membrane modified by reduced graphene oxide/TiO2 with improved desalination performance.* Journal of Membrane Science, 2015. **489**: p. 43-54.

52. Uemura, T., et al., *Membrane technology in seawater desalination: History, recent developments and future prospects.* Desalination and Water Treatment, 2011. **33**(1-3): p. 283-288.

53. Tan, C.H. and H.Y. Ng, *Modified models to predict flux behavior in forward osmosis in consideration of external and internal concentration polarizations.* Journal of Membrane Science, 2008. **324**(1-2): p. 209-219.

54. Lutchmiah, K., et al., *Water recovery from sewage using forward osmosis.* Water Science and Technology, 2011. **64**(7): p. 1443-1449.

55. Kargol, M. and A. Kargol, *Membrane transport generated by the osmotic and hydrostatic pressure. Correlation relation for parameters L-p, sigma, and omega.* Journal of Biological Physics, 2000. **26**(4): p. 307-320.

56. Marvel, S.C. and M.V. Kepler, *A Simple Membrane Osmometer System & Experiments That Quantitatively Measure Osmotic Pressure.* American Biology Teacher, 2009. **71**(6): p. 355-362.

57. Ohashi, H., N. Miyaoi, and T. Yamaguchi, *Osmotic pressure expression with several guest ions on a molecular recognition ion gating membrane.* Journal of Photopolymer Science and Technology, 2006. **19**(2): p. 251-252.

58. Kim, H., J.S. Choi, and S. Lee, *Pressure retarded osmosis for energy production: membrane materials and operating conditions.* Water Science and Technology, 2012. **65**(10): p. 1789-1794.

59. Lin, S.H., et al., *Hybrid Pressure Retarded Osmosis-Membrane Distillation System for Power Generation from Low-Grade Heat: Thermodynamic Analysis and Energy Efficiency.* Environmental Science & Technology, 2014. **48**(9): p. 5306-5313.

60. He, W., Y. Wang, and M.H. Shaheed, *Enhanced energy generation and membrane performance by two-stage pressure retarded osmosis (PRO).* Desalination, 2015. **359**: p. 186-199.

61. You, Y.H., et al., *Semipermeable Membrane Mass Transfer in Pressure-Retarded Osmosis Process.* Advances in Computer Science and Engineering, 2012. **141**: p. 307-315.

62. Yip, N.Y., et al., *Thin-Film Composite Pressure Retarded Osmosis Membranes for Sustainable Power Generation from Salinity Gradients.* Environmental Science & Technology, 2011. **45**(10): p. 4360-4369.

63.	Kotsanopoulos, K.V. and I.S. Arvanitoyannis, *Membrane Processing Technology in the Food Industry: Food Processing, Wastewater Treatment, and Effects on Physical, Microbiological, Organoleptic, and Nutritional Properties of Foods.* Critical Reviews in Food Science and Nutrition, 2015. **55**(9): p. 1147-1175.

64.	Kim, Y.C. and M. Elimelech, *Potential of osmotic power generation by pressure retarded osmosis using seawater as feed solution: Analysis and experiments.* Journal of Membrane Science, 2013. **429**: p. 330-337.

65.	Klaysom, C., et al., *Forward and pressure retarded osmosis: potential solutions for global challenges in energy and water supply.* Chemical Society Reviews, 2013. **42**(16): p. 6959-6989.

66.	Ge, Q.C., M.M. Ling, and T.S. Chung, *Draw solutions for forward osmosis processes: Developments, challenges, and prospects for the future.* Journal of Membrane Science, 2013. **442**: p. 225-237.

67.	Zhao, S.F., et al., *Recent developments in forward osmosis: Opportunities and challenges.* Journal of Membrane Science, 2012. **396**: p. 1-21.

68.	Dreyer, D.R., et al., *The chemistry of graphene oxide.* Chemical Society Reviews, 2010. **39**(1): p. 228-240.

69.	Hofmann, U., and Rudolf Holst, *Über die Säurenatur und die Methylierung von Graphitoxyd.* Berichte der deutschen chemischen Gesellschaft (A and B Series), 1939. **72.4 (1939)**: p. 18.

70.	Hofmann, U., et al., *Die Struktur Und Die Graphitierung Von Kohlenstoff.* Zeitschrift Fur Anorganische Chemie, 1947. **255**(1-3): p. 195-211.

71.	Scholz, W. and H.P. Boehm, *Graphite Oxide .6. Structure of Graphite Oxide.* Zeitschrift Fur Anorganische Und Allgemeine Chemie, 1969. **369**(3-6): p. 327-&.

72.	He, H.Y., et al., *A new structural model for graphite oxide.* Chemical Physics Letters, 1998. **287**(1-2): p. 53-56.

73.	Zhu, Y.W., et al., *Graphene and Graphene Oxide: Synthesis, Properties, and Applications.* Advanced Materials, 2010. **22**(35): p. 3906-3924.

74.	Rodriguez-Pastor, I., et al., *Towards the understanding of the graphene oxide structure: How to control the formation of humic- and fulvic-like oxidized debris.* Carbon, 2015. **84**: p. 299-309.

75.	Nair, R.R., et al., *Unimpeded Permeation of Water Through Helium-Leak-Tight Graphene-Based Membranes.* Science, 2012. **335**(6067): p. 442-444.

76.	Joshi, R.K., et al., *Precise and Ultrafast Molecular Sieving Through Graphene Oxide Membranes.* Science, 2014. **343**(6172): p. 752-754.

77.	Mi, B.X., *Graphene Oxide Membranes for Ionic and Molecular Sieving.* Science, 2014. **343**(6172): p. 740-742.

78.	Algara-Siller, G., et al., *Square ice in graphene nanocapillaries.* Nature, 2015. **519**(7544): p. 443-+.

79.	Hegab, H.M., et al., *Improving the fouling resistance of brackish water membranes via surface modification with graphene oxide functionalized chitosan.* Desalination, 2015. **365**: p. 99-107.

80. Hu, M. and B.X. Mi, *Layer-by-layer assembly of graphene oxide membranes via electrostatic interaction.* Journal of Membrane Science, 2014. **469**: p. 80-87.

81. Bano, S., et al., *Graphene oxide modified polyamide nanofiltration membrane with improved flux and antifouling properties.* Journal of Materials Chemistry A, 2015. **3**(5): p. 2065-2071.

82. Perry, G., et al., *Investigation of the anti-biofouling properties of graphene oxide aqueous solutions by electrowetting characterization.* Journal of Materials Chemistry A, 2013. **1**(39): p. 12355-12360.

83. Perry, G., et al., *Inhibiting protein biofouling using graphene oxide in droplet-based microfluidic microsystems.* Lab on a Chip, 2012. **12**(9): p. 1601-1604.

84. Jung, H., et al., *Preparation of PvdF nanofiber/magnetite graphene oxide composite membrane and its arsenic removal property.* Abstracts of Papers of the American Chemical Society, 2013. **246**.

85. Mishra, A.K. and S. Ramaprabhu, *Functionalized graphene sheets for arsenic removal and desalination of sea water.* Desalination, 2011. **282**: p. 39-45.

86. Chen, J.M., et al., *Preparation and evaluation of graphene-coated solid-phase microextraction fiber.* Analytica Chimica Acta, 2010. **678**(1): p. 44-49.

87. Liang, H., X.J. Miao, and J.M. Gong, *One-step fabrication of layered double hydroxides/graphene hybrid as solid-phase extraction for stripping voltammetric detection of methyl parathion.* Electrochemistry Communications, 2012. **20**: p. 149-152.

88. Liu, X.T., et al., *Graphene-coated silica as a highly efficient sorbent for residual organophosphorus pesticides in water.* Journal of Materials Chemistry A, 2013. **1**(5): p. 1875-1884.

89. Thinh, P.X., et al., *Fabrication and characterization of honeycomb-patterned film from poly(epsilon-caprolactone)/poly((R)-3-hydroxybutyric acid)/reduced graphene oxide composite.* Polymer Journal, 2013. **45**(10): p. 1064-1071.

90. Sinha, A. and N.R. Jana, *Graphene-Based Composite with gamma-Fe2O3 Nanoparticle for the High-Performance Removal of Endocrine-Disrupting Compounds from Water.* Chemistry-an Asian Journal, 2013. **8**(4): p. 786-791.

91. Yu, Y. and L.S. Wu, *Application of graphene for the analysis of pharmaceuticals and personal care products in wastewater.* Analytical and Bioanalytical Chemistry, 2013. **405**(14): p. 4913-4919.

92. Zhang, Y.L., et al., *Adsorption of Clofibric Acid from Aqueous Solution by Graphene Oxide and the Effect of Environmental Factors.* Water Air and Soil Pollution, 2014. **225**(8).

93. Hu, M. and B.X. Mi, *Enabling Graphene Oxide Nanosheets as Water Separation Membranes.* Environmental Science & Technology, 2013. **47**(8): p. 3715-3723.

94. Zhao, J., et al., *Fabricating graphene oxide-based ultrathin hybrid membrane for pervaporation dehydration via layer-by-layer self-assembly driven by multiple interactions.* Journal of Membrane Science, 2015. **487**: p. 162-172.

95. Choi, W., et al., *Layer-by-Layer Assembly of Graphene Oxide Nanosheets on Polyamide Membranes for Durable Reverse-Osmosis Applications.* Acs Applied Materials & Interfaces, 2013. **5**(23): p. 12510-12519.

96.   de Grooth, J., et al., *The role of ionic strength and odd-even effects on the properties of polyelectrolyte multilayer nanofiltration membranes.* Journal of Membrane Science, 2015. **475**: p. 311-319.

97.   Schonbeck, N., et al., *Surfactant-Triggered Disassembly of Electrostatic Complexes Probed at Optical and Quartz Crystal Microbalance Length Scales.* Langmuir, 2014. **30**(19): p. 5620-5627.

98.   Park, S., et al., *Graphene Oxide Sheets Chemically Cross-Linked by Polyallylamine.* Journal of Physical Chemistry C, 2009. **113**(36): p. 15801-15804.

99.   Cui, W., et al., *A Strong Integrated Strength and Toughness Artificial Nacre Based on Dopamine Cross-Linked Graphene Oxide.* Acs Nano, 2014. **8**(9): p. 9511-9517.

100.   Ha, H., K. Shanmuganathan, and C.J. Ellison, *Mechanically Stable Thermally Cross linked Poly(acrylic acid)/Reduced Graphene Oxide Aerogels.* Acs Applied Materials & Interfaces, 2015. **7**(11): p. 6220-6229.

101.   Dikin, D.A., et al., *Preparation and characterization of graphene oxide paper.* Nature, 2007. **448**(7152): p. 457-460.